Electronic Supplementary Material (ESI) for Dalton Transactions.

Supporting Information

White Light *and* Colour-Tunable Emission from a Single Component Europium-1,8-Naphthalimide Thin Film

Alex T. O'Neil[a], Anaïs Chalard[b], Jenny Malmström[b], and Jonathan A. Kitchen*[a]

a. School of Natural Sciences, Massey University, Auckland, New Zealand.
b. Department of Chemical and Materials Engineering, University of Auckland, Auckland 1142, New Zealand

Table of contents

Section 1 - Ligand Characterisation Data

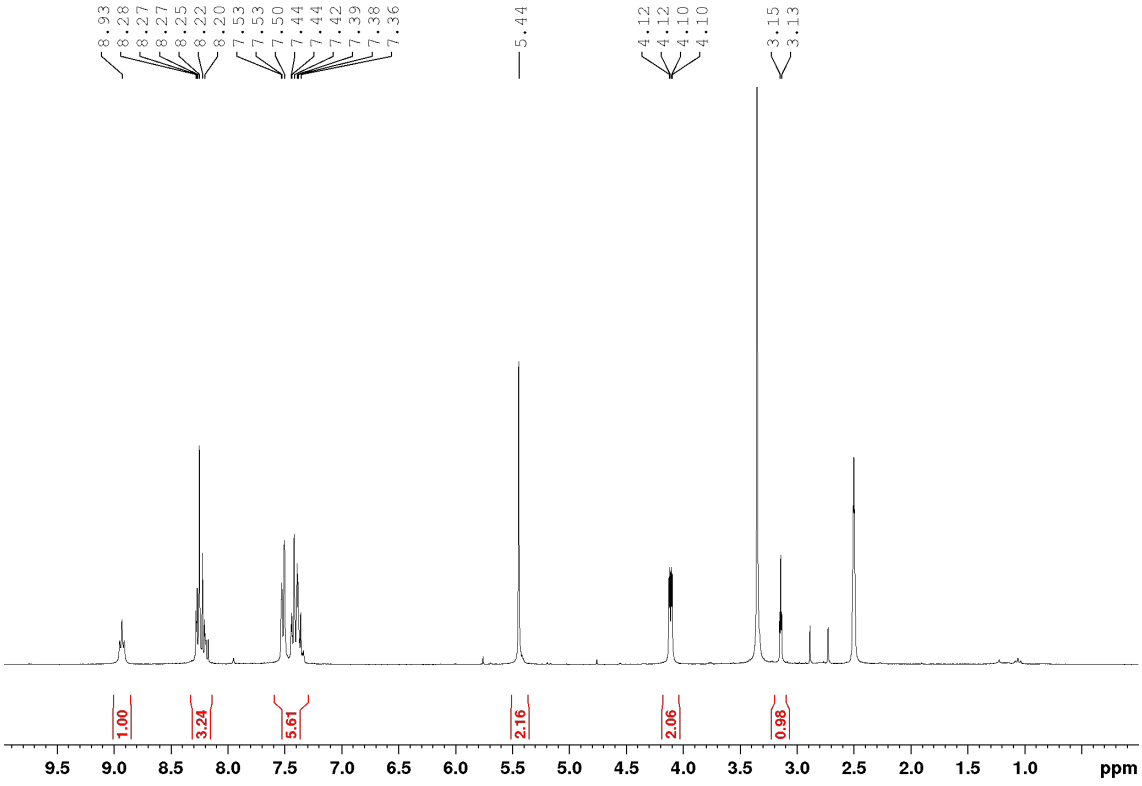

Figure S1. ^{1}H NMR spectrum (300 MHz, DMSO-d_6) of **A**.

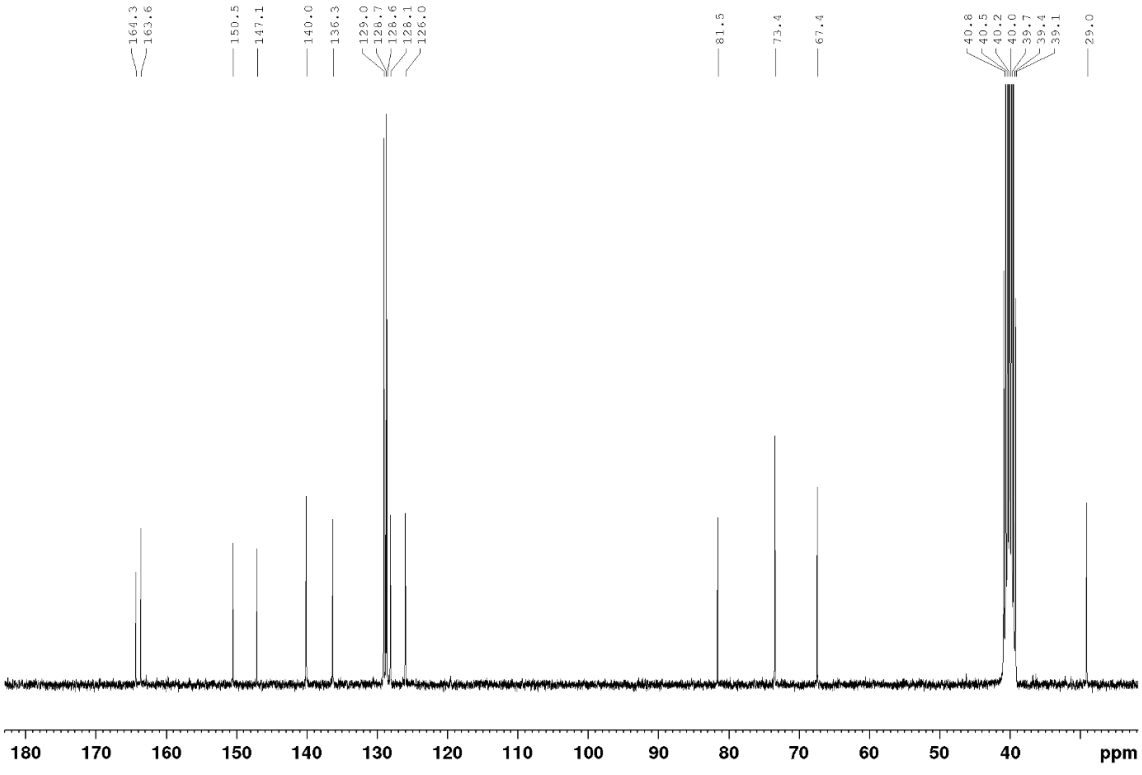

Figure S2. ^{13}C NMR spectrum (75 MHz, DMSO-d_6) of **A**.

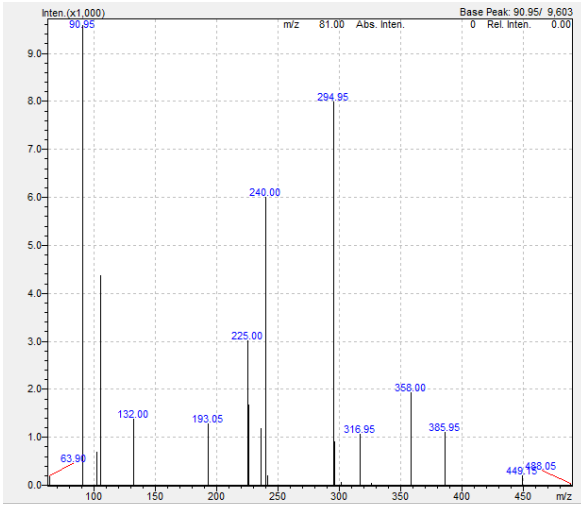

Figure S3. LRMS m/z = 294.95 [**A** + H]$^+$ (calc. for $C_{17}H_{15}N_2O_3^+$, 295.11), m/z = 316.95 [**A** + H]$^+$ (calc. for $C_{17}H_{15}N_2O_3^+$, 317.19)

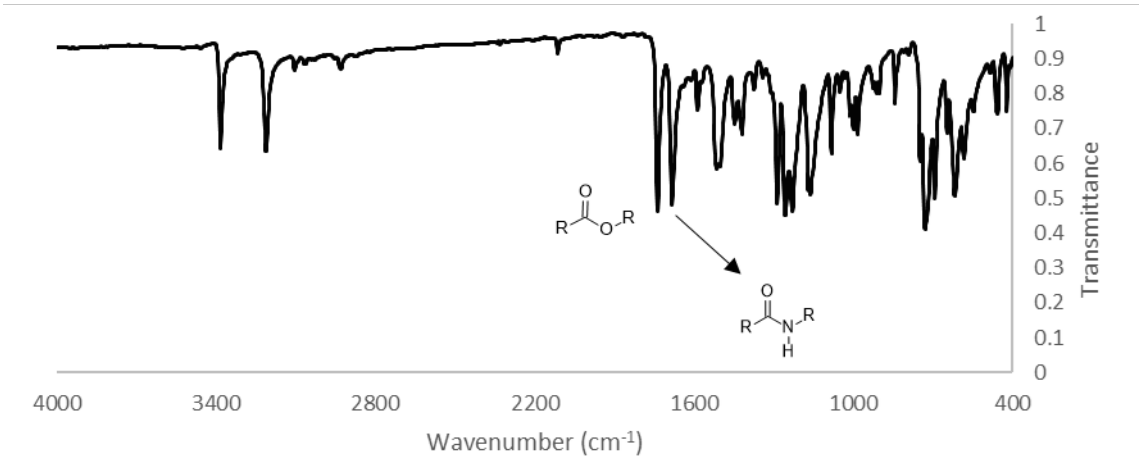

Figure S4 IR spectrum of **A**.

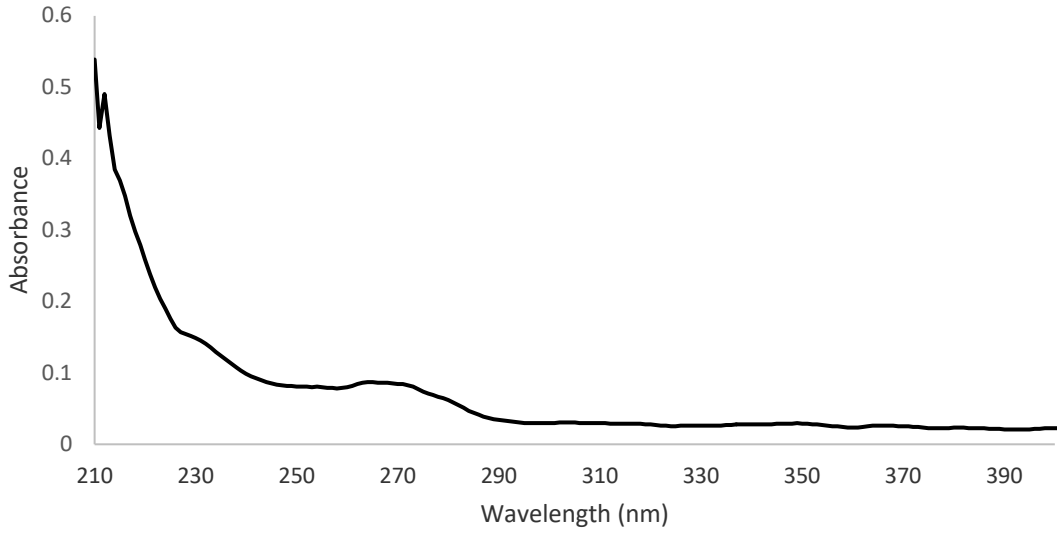

Figure S5. UV-visible absorption spectrum of **A** (0.01 mM, MeOH).

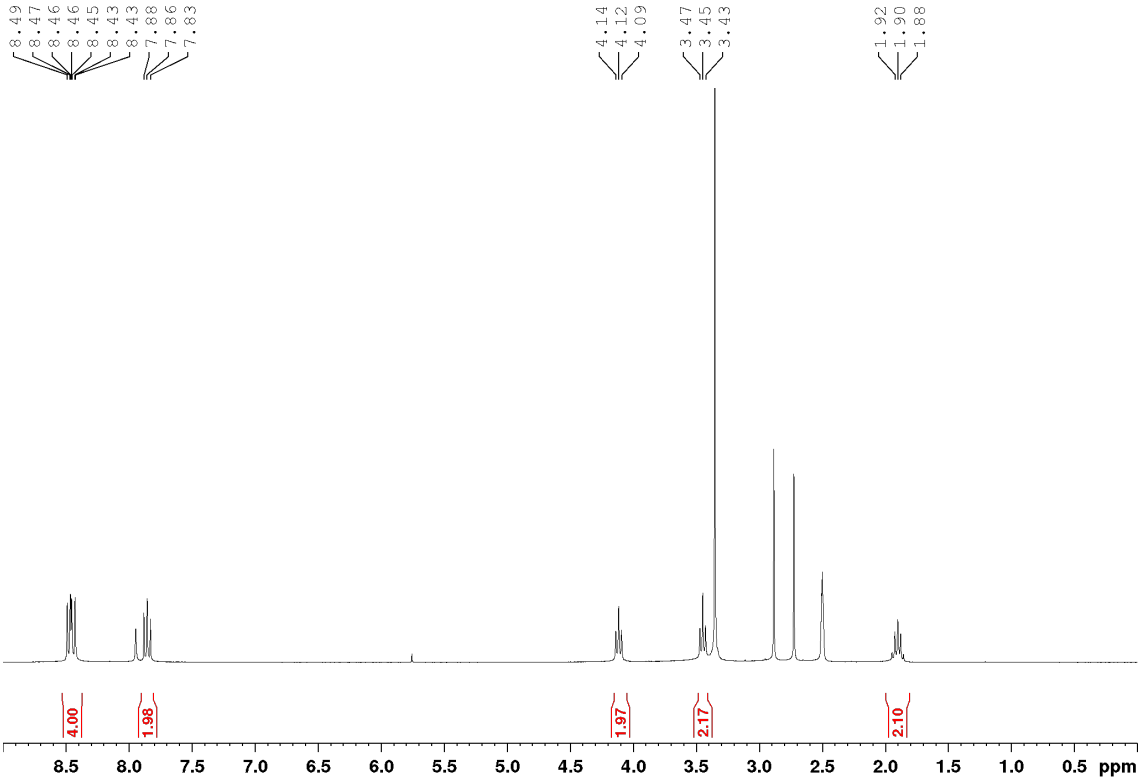

Figure S6. *^{1}H NMR spectrum (300 MHz, DMSO-d_6) of **B**.*

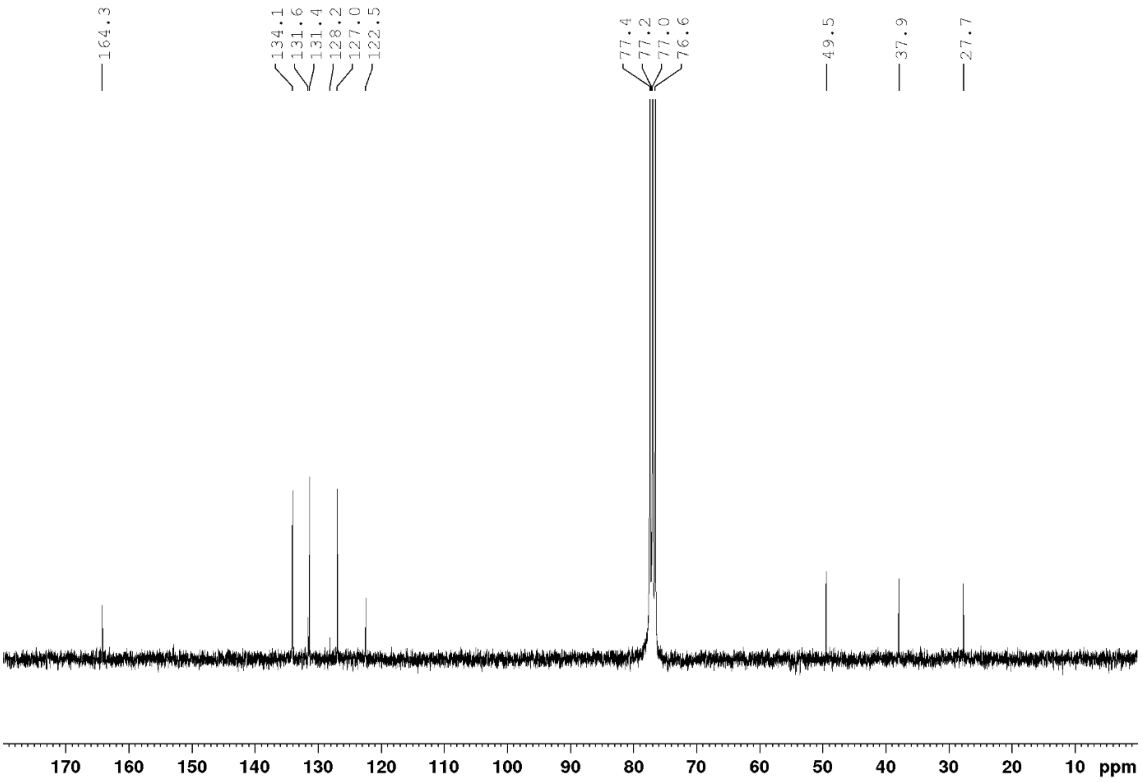

Figure S7. *^{13}C NMR spectrum (75 MHz, DMSO-d_6) of **B**.*

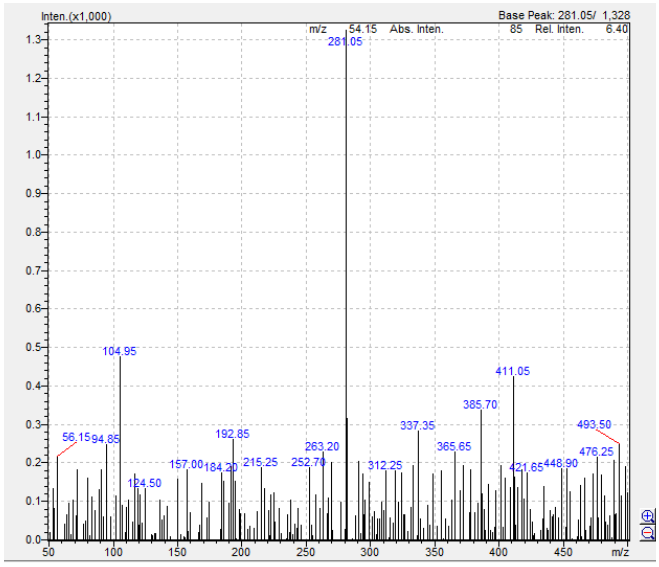

Figure S8. *LRMS m/z = 281.05 [B + H]⁺ (calc. for $C_{15}H_{12}N_4O_2^+$, 281.10).*

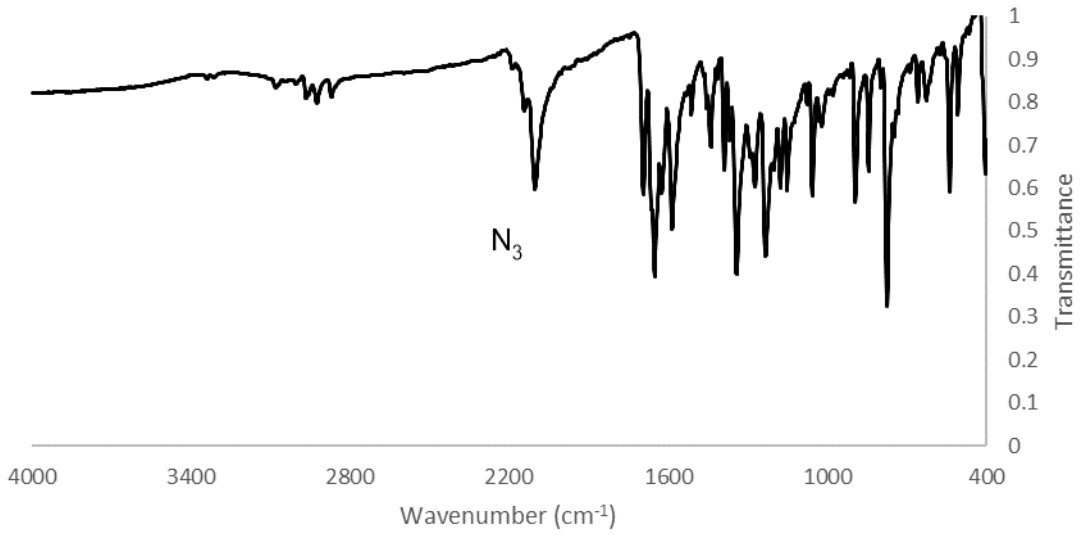

Figure S9. *IR spectrum of **B**.*

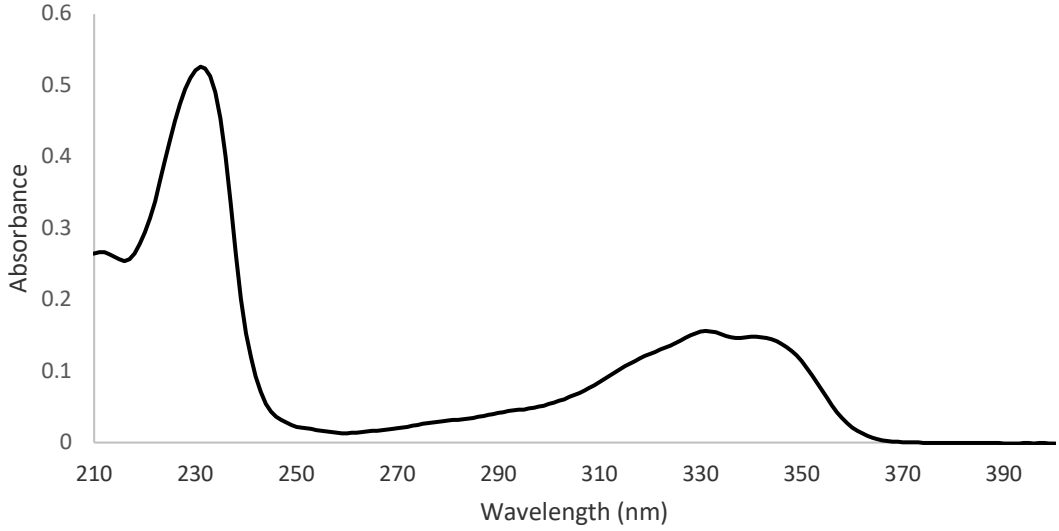

Figure S10. *UV-visible absorption spectrum of **B** (0.01 mM, MeOH).*

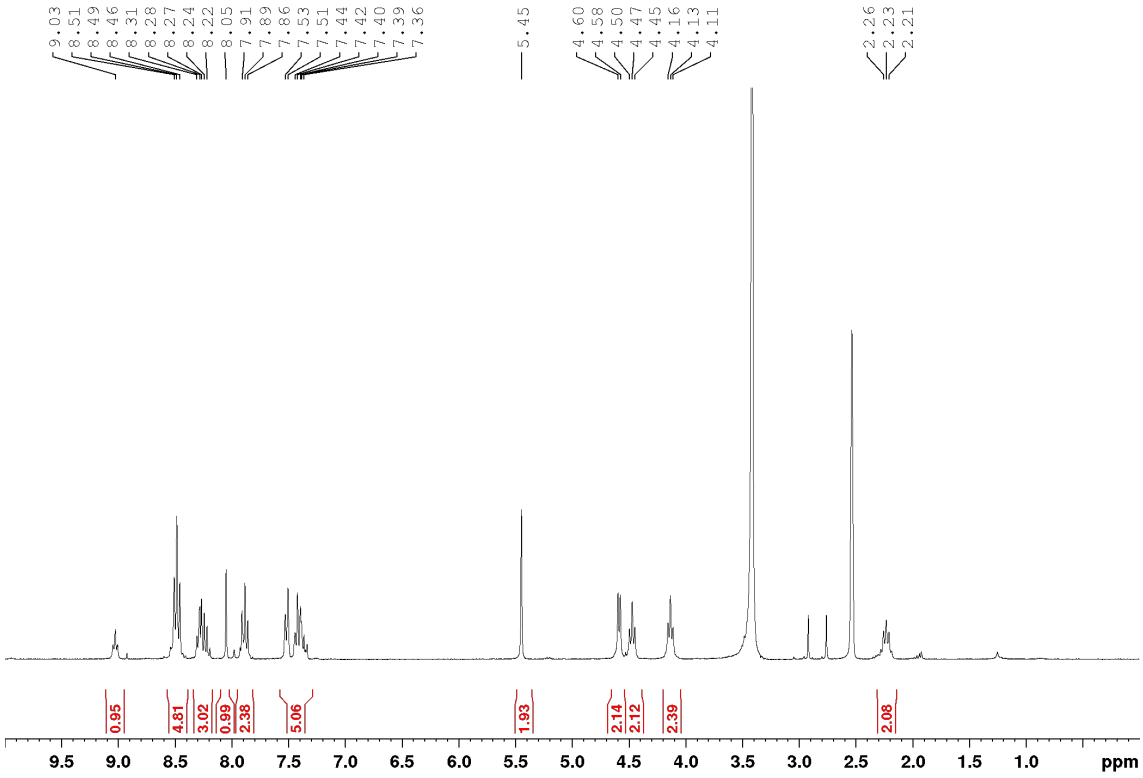

Figure S11. ^{1}H NMR spectrum (300 MHz, DMSO-d_6) of **1Bz**.

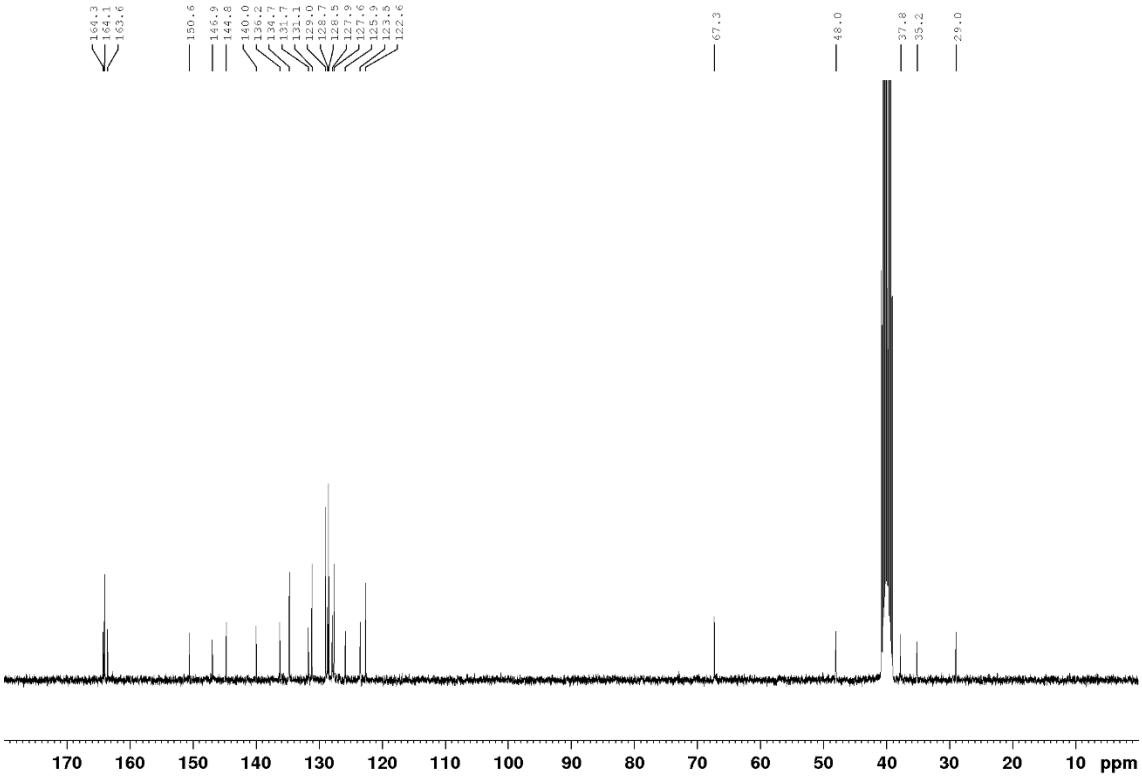

Figure S12. ^{13}C NMR spectrum (75 MHz, DMSO-d_6) of **1Bz**.

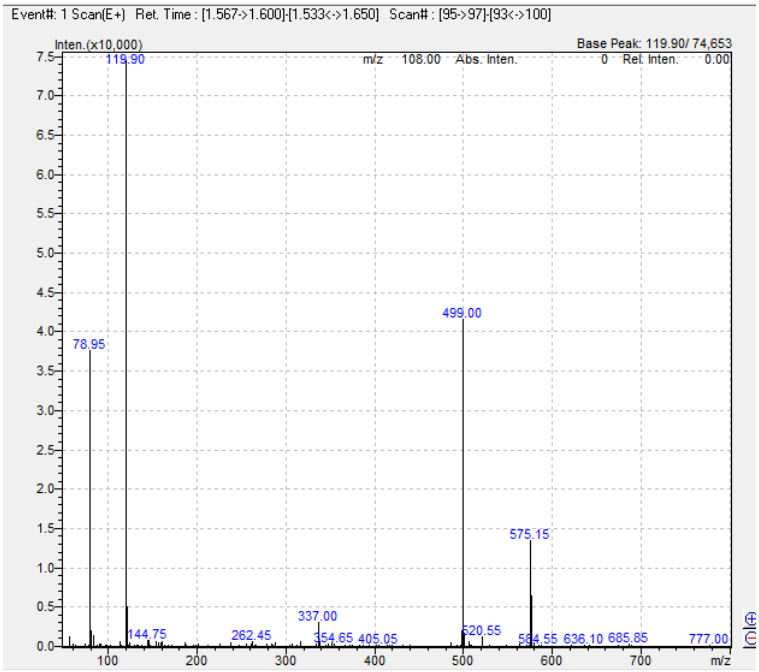

Figure S13. LRMS m/z = 575.15 [**1Bz** + H]$^+$ (calc. for $C_{32}H_{27}N_6O_5^+$, 575.20).

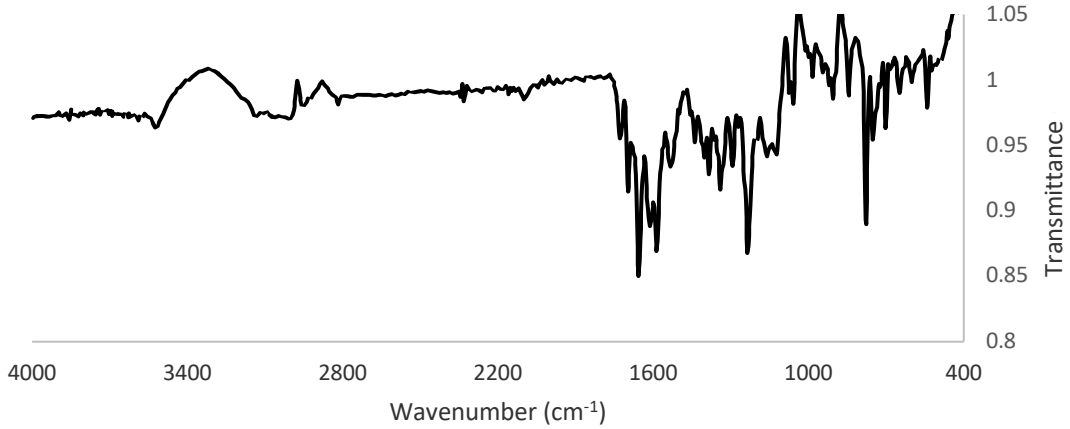

Figure S14. IR spectrum of **1Bz**.

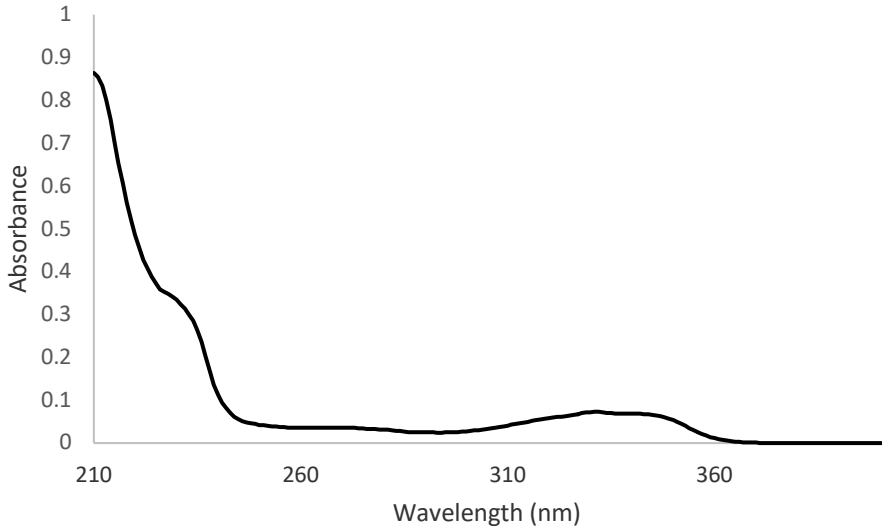

Figure S15. UV-visible absorption spectrum of **1Bz** (0.01 mM, MeOH).

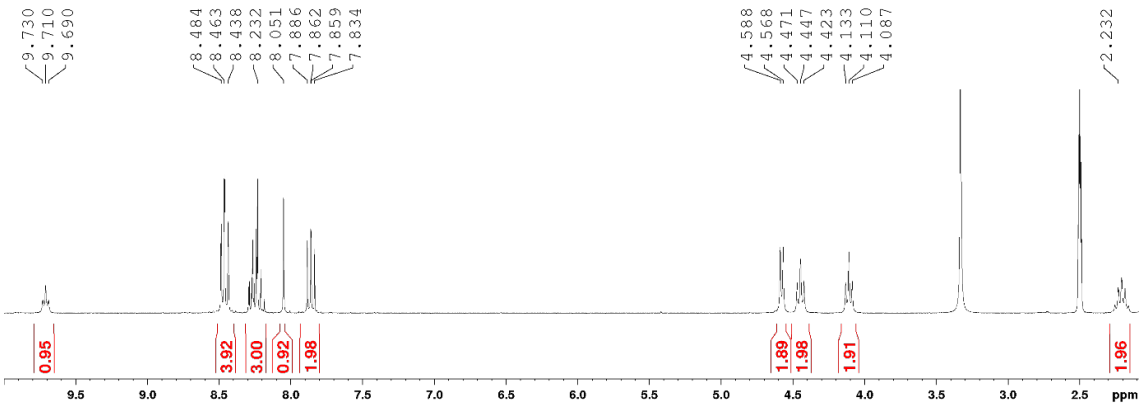

Figure S16. ^{1}H NMR spectrum (300 MHz, DMSO-d_6) of **1H**.

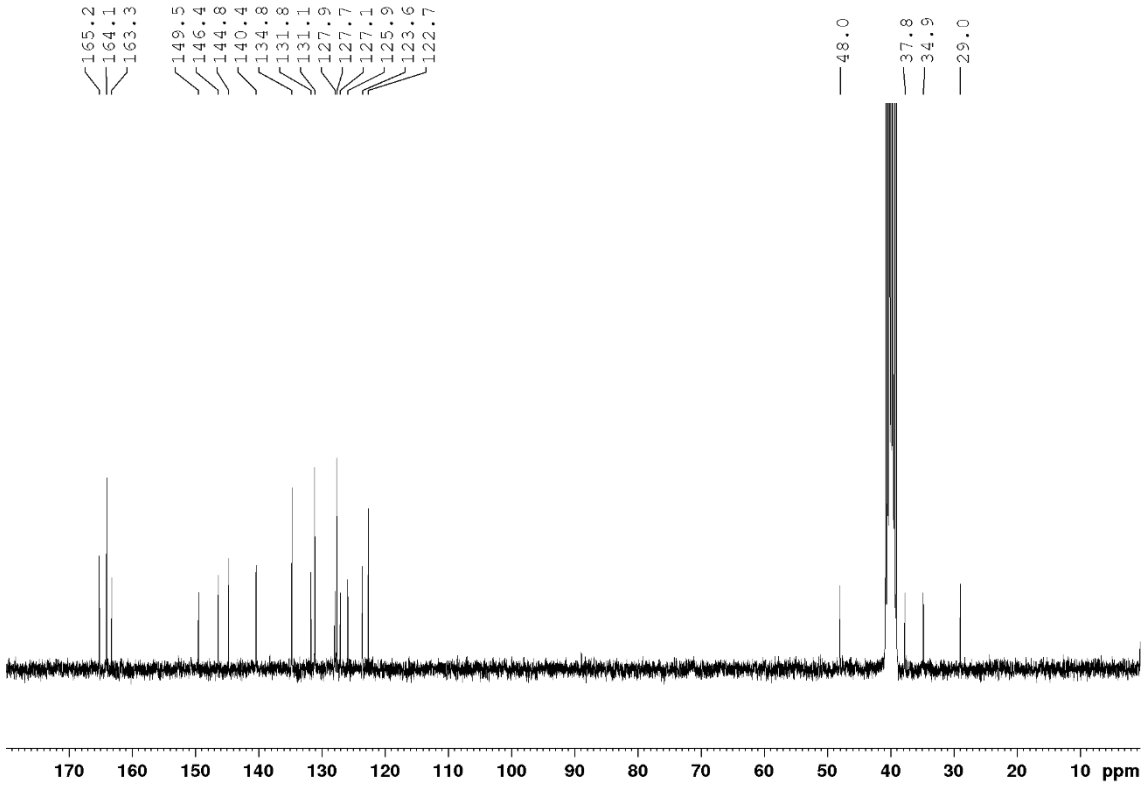

Figure S17. ^{13}C NMR spectrum (75 MHz, DMSO-d_6) of **1H**.

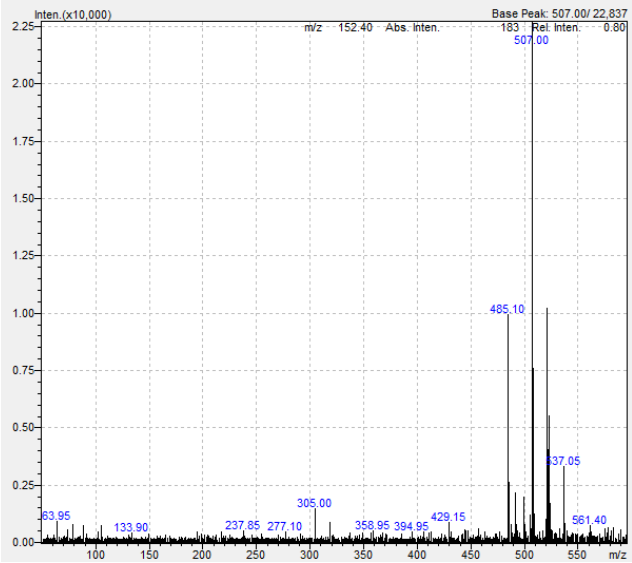

Figure S18. LRMS m/z = 485.10 [**1H** + H]$^+$ (calc. for $C_{25}H_{21}N_6O_5^+$, 485.16) and m/z = 507.00 [**1H** + Na]$^+$ (calc. for $C_{25}H_{20}N_6O_5Na^+$, 507.14).

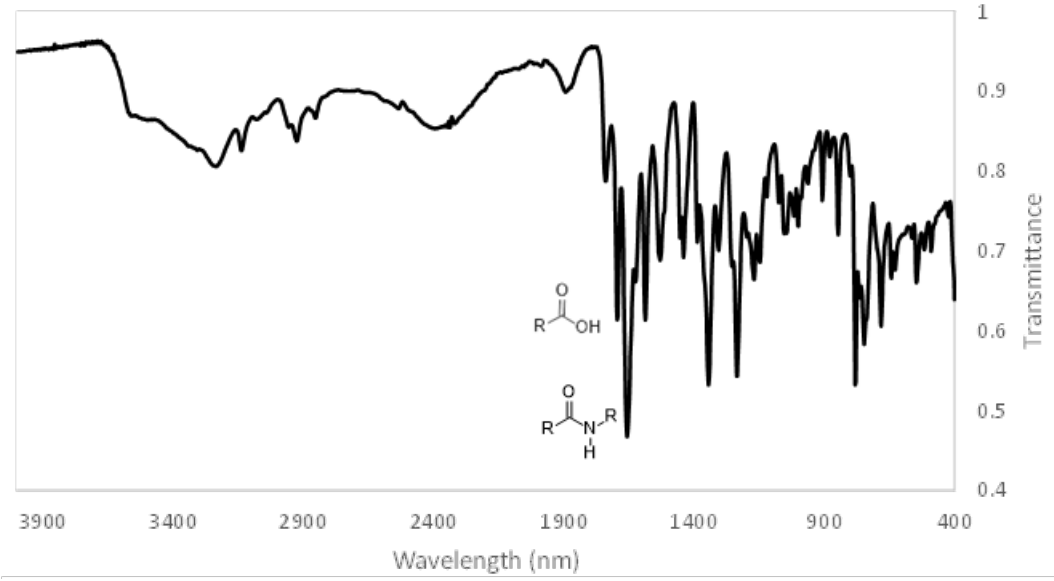

Figure S19. IR spectrum of **1H**.

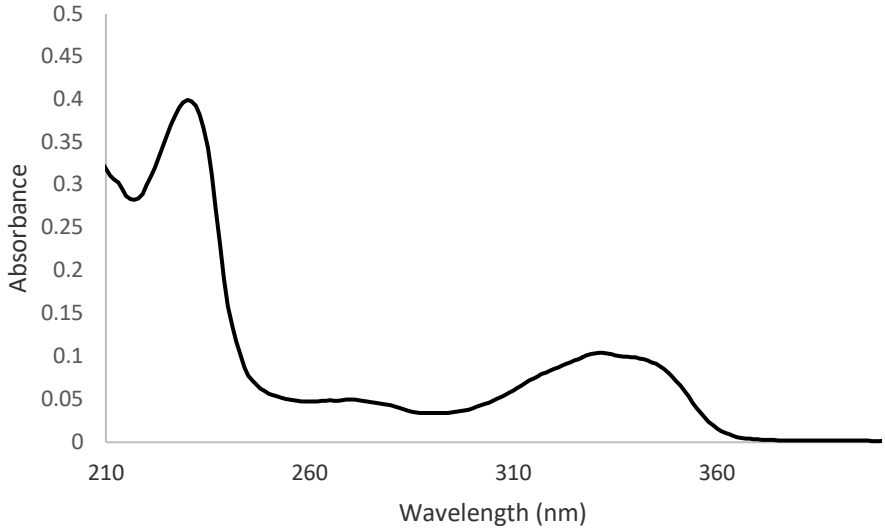

Figure S20. UV-visible absorption spectrum of **1H** (0.01 mM, MeOH).

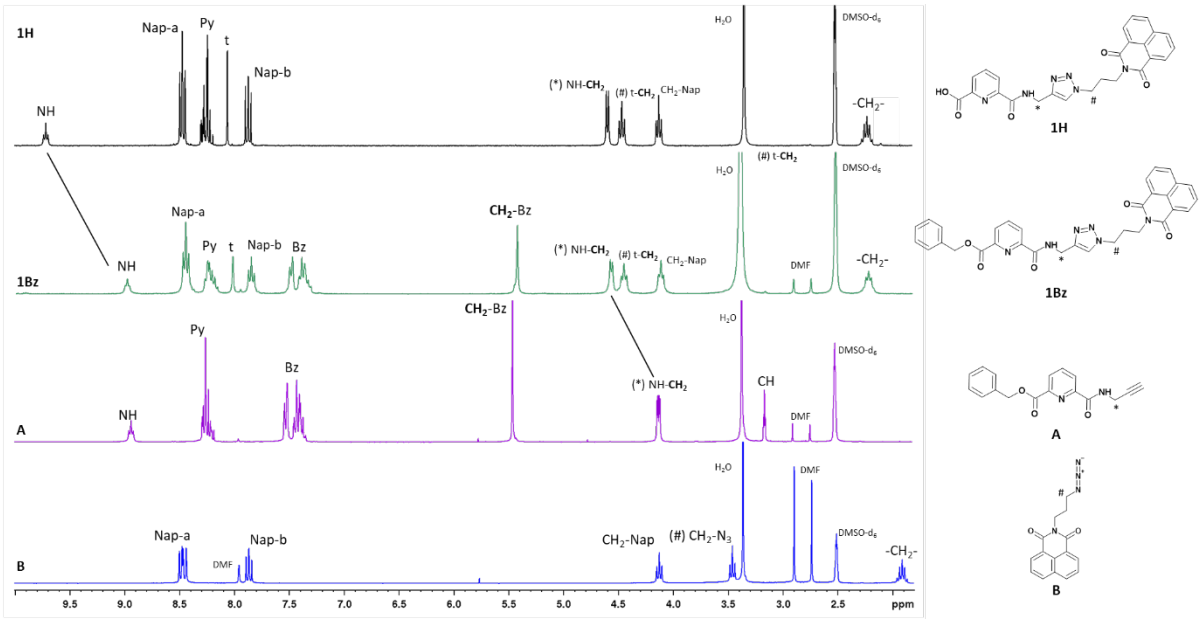

Figure S21. ^{1}H NMR of **1H**, **1Bz**, **A** and **B** (300 MHz, DMSO-d_6). Abbreviations: Nap-a for ortho and para protons of **Nap**, Nap-b for meta protons of **Nap**, Py for pyridine ring, t for 1, 2,3-triazole, and Bz for benzyl ring. CH_2 in bold indicates methylene associated with the signal.

Section 2 - Lanthanide Complex Characterisation

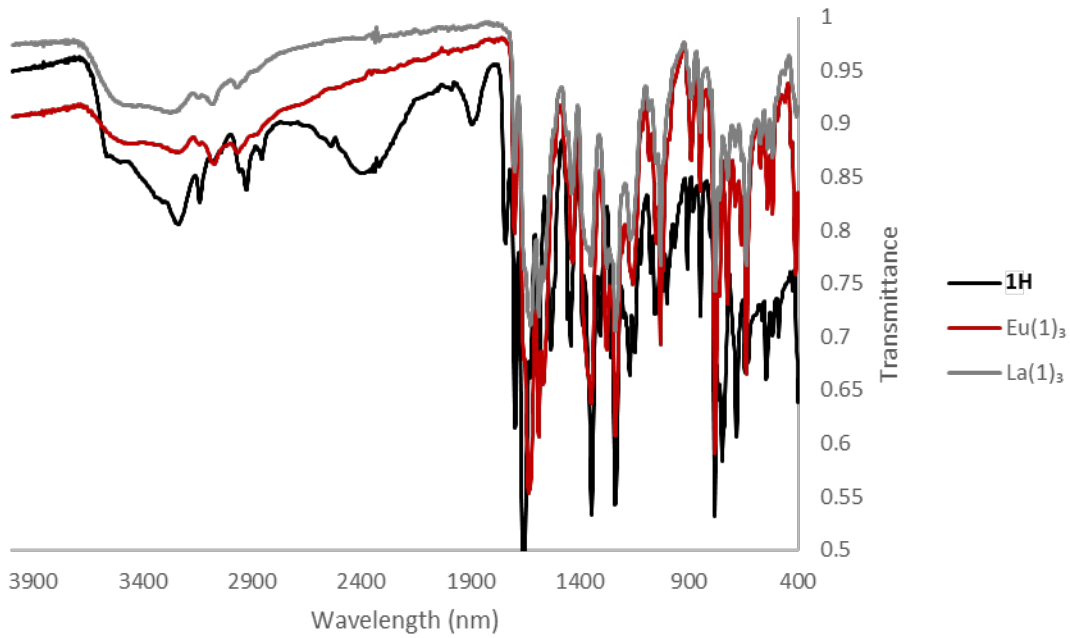

Figure S22. IR spectra of **1H,** Eu(**1**)$_3$ and La(**1**)$_3$.

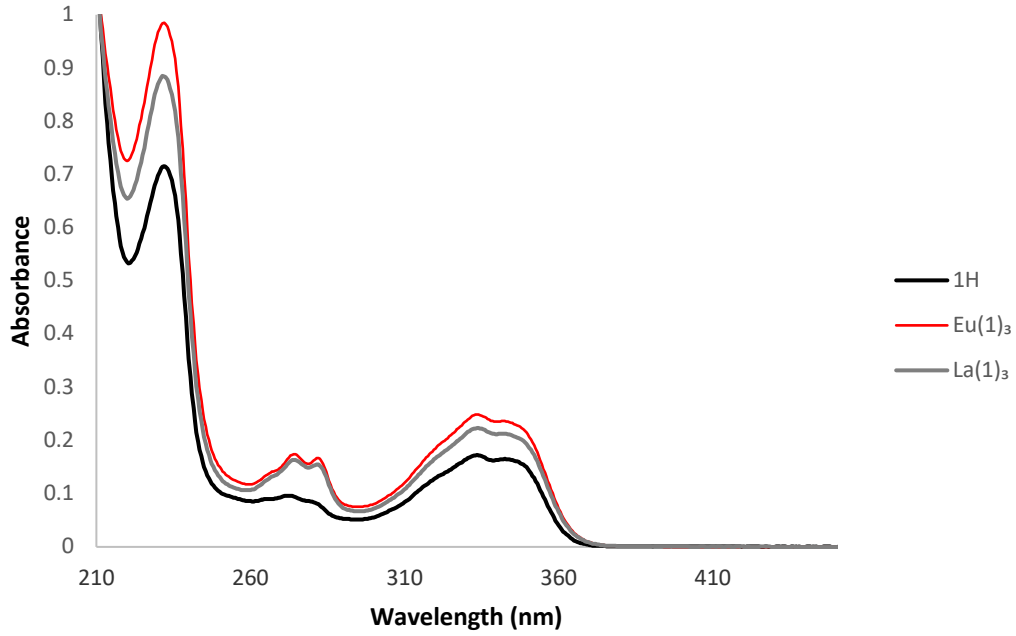

Figure S23. UV-visible absorption of **1H,** Eu(**1**)$_3$ and La(**1**)$_3$ (0.01 mM, MeOH).

Eu(1)$_3$

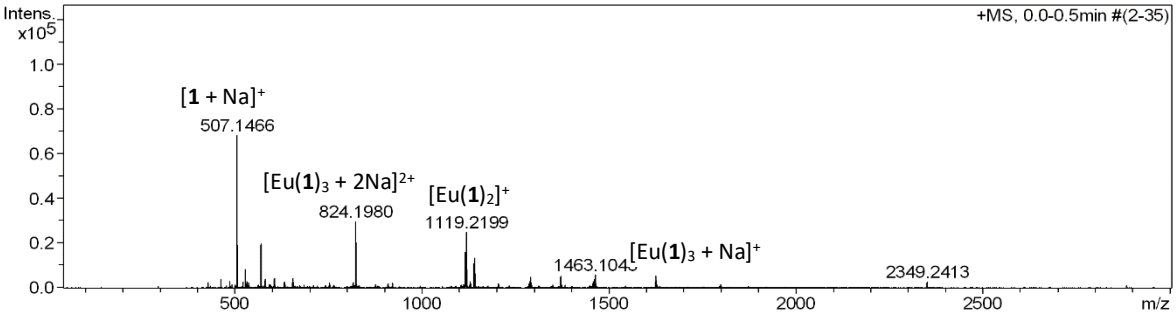

***Figure S24**. HRMS Eu(**1**)$_3$.*

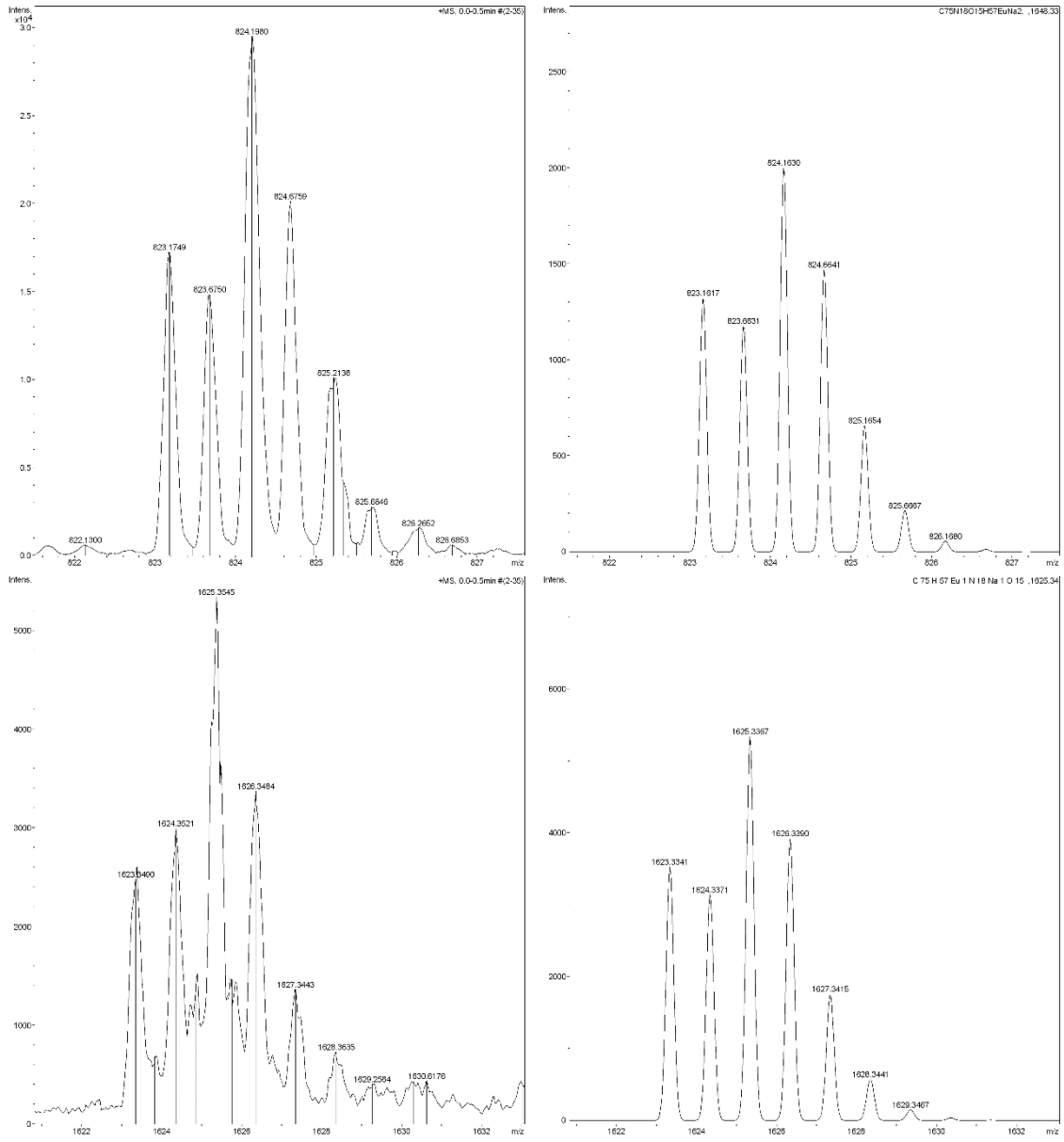

***Figure S25**. (Top left) HRMS m/z = 824.1980 [Eu(**1**)$_3$ + 2Na]$^{2+}$. (Top right) Calc. for ($C_{75}H_{57}N_{18}O_{15}EuNa_2$)$^{2+}$, 824.1630. (Bottom left) HRMS m/z = 1625.3545 [Eu(**1**)$_3$ + Na]$^+$. (Bottom right) Calc. for ($C_{75}H_{57}N_{18}O_{15}EuNa$)$^+$, 1625.3367.*

La(1)$_3$

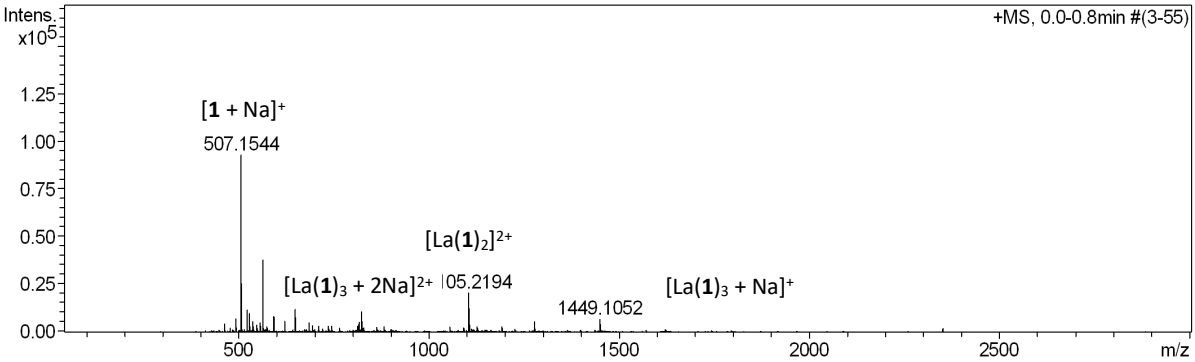

***Figure S26**. HRMS La(**1**)$_3$.*

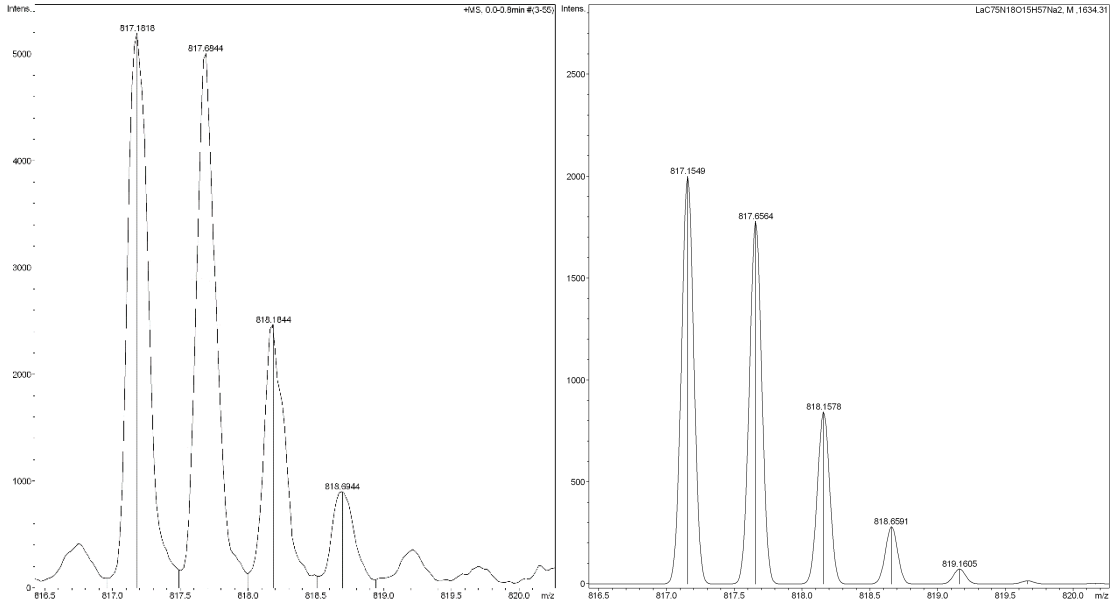

***Figure S27**. (Left) HRMS m/z = 817.1818 [La(**1**)$_3$ + 2Na]$^{2+}$. (Right) Calc. for ($C_{75}H_{57}N_{18}O_{15}LaNa_2$)$^{2+}$, 817.1549.*

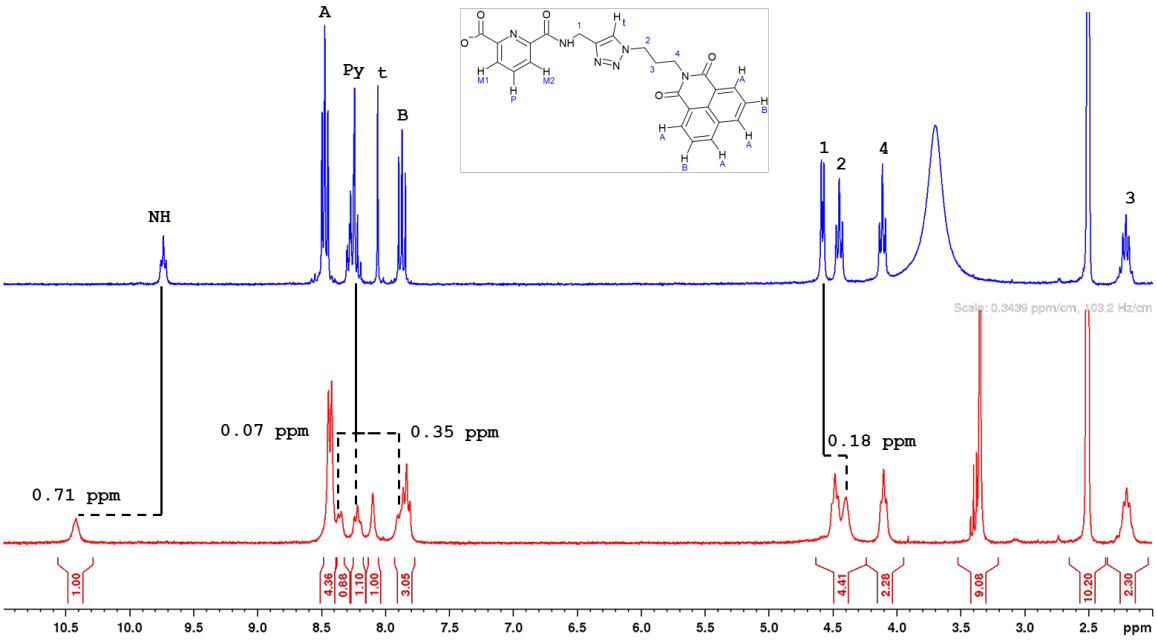

Figure S28. ^{1}H NMR spectrum (300 MHz, DMSO-d_6) of La(**1**)$_3$ (bottom) and **1H** (top). ^{1}H NMR of La(**1**)$_3$ shows significant downfield shift in the NH signal (0.71 ppm) and a corresponding upfield shift in the methylene linker (**CH$_2$**-NH, 0.18 ppm), previously observed in similar PDC systems indicative of La^{3+} coordination in the NO_2 pocket. Additionally, the pyridyl aromatic proton signals experienced shifts resulting in the single multiplet pyridyl signal in **1H** splitting into three separate distinct signals, which is suggestive of overall C_3 symmetry within the La^{3+} coordination sphere.

Section 3 - Photophysical Properties of 1H, $Eu(1)_3$ and $La(1)_3$

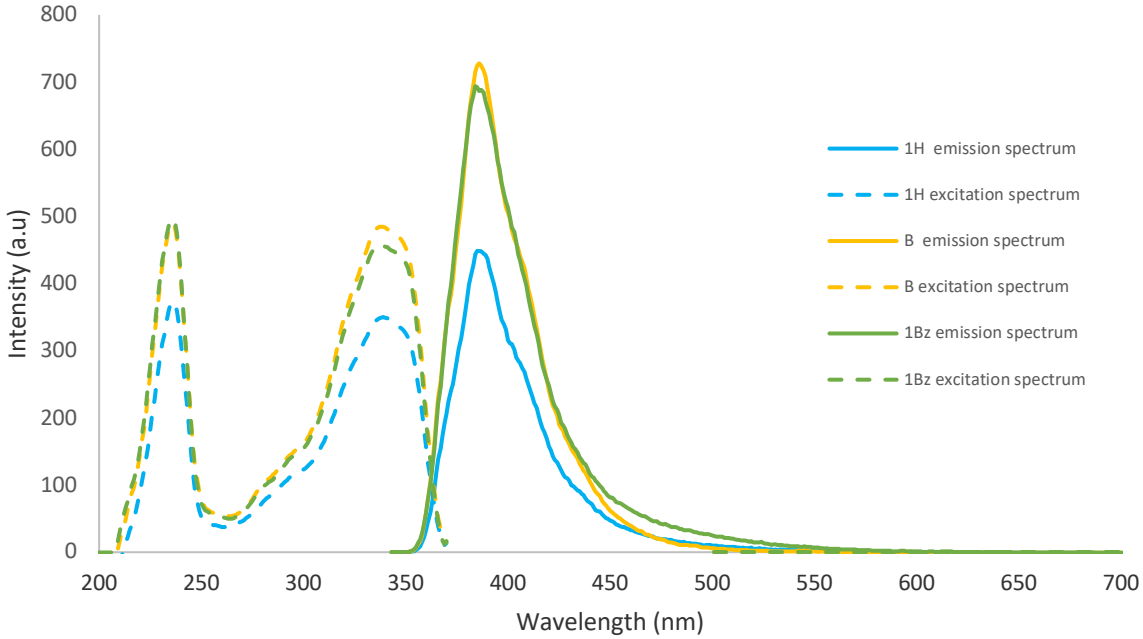

***Figure S29**. Fluorescent emission (λ_{ex} =340 nm) and excitation spectra (λ =390 nm) spectra of Ligand **1H**, intermediate **C** and precursor **B** (0.01 mM, MeOH)*

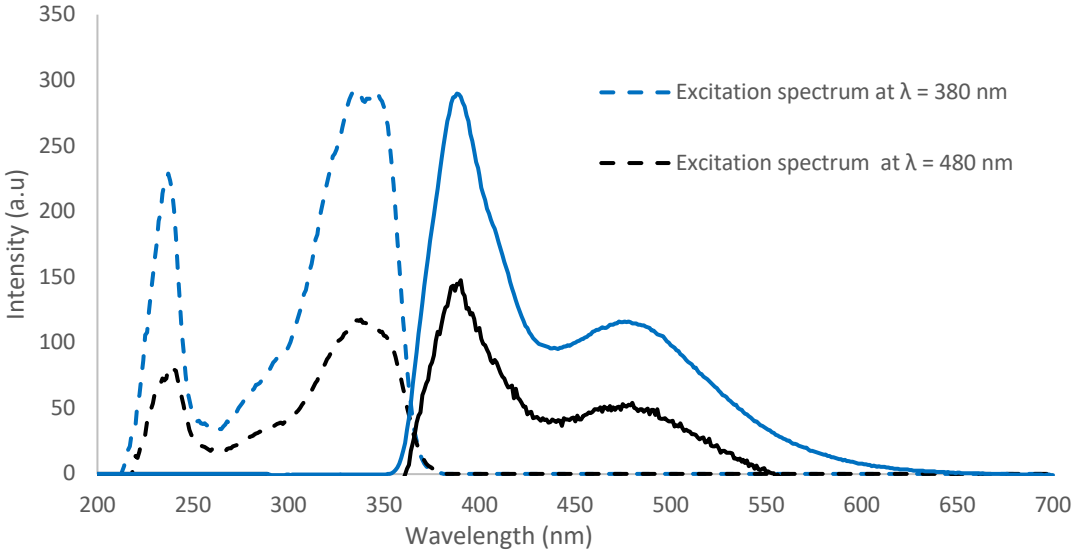

Figure S30. $La(\mathbf{1})_3$ fluorescence spectra (0.01 mM, MeOH).

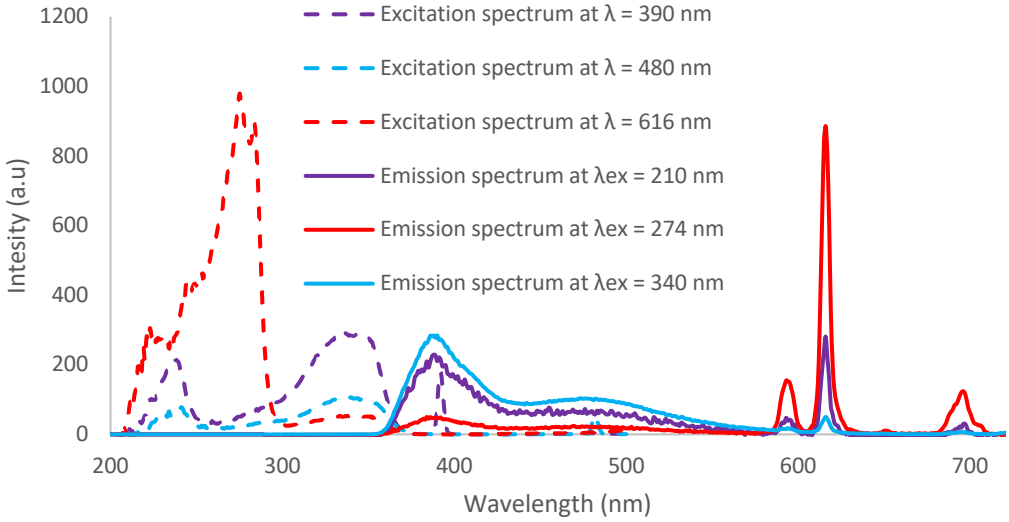

Figure S31. Eu(**1**)$_3$ fluorescence spectra (0.01 mM, MeOH).

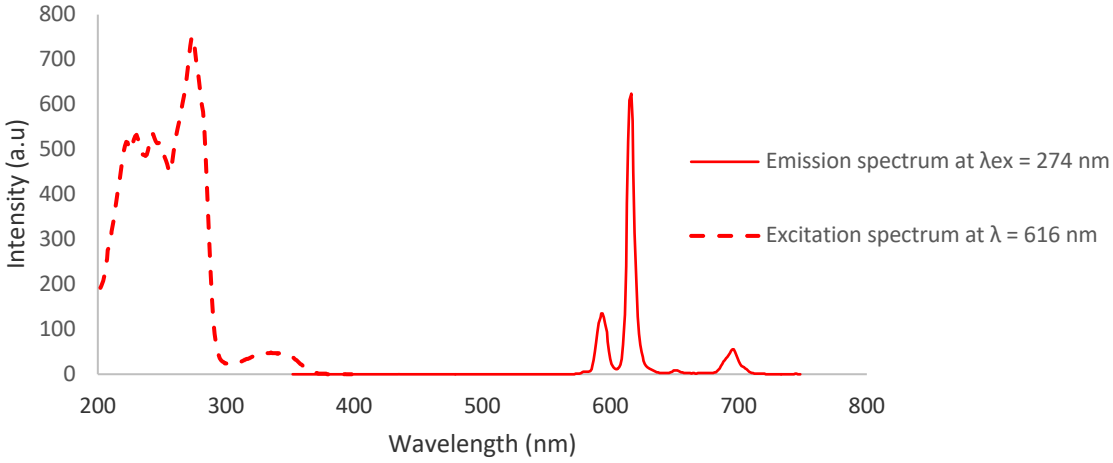

Figure S32. Eu(**1**)$_3$ phosphorescence spectrum (0.01 mM, MeOH).

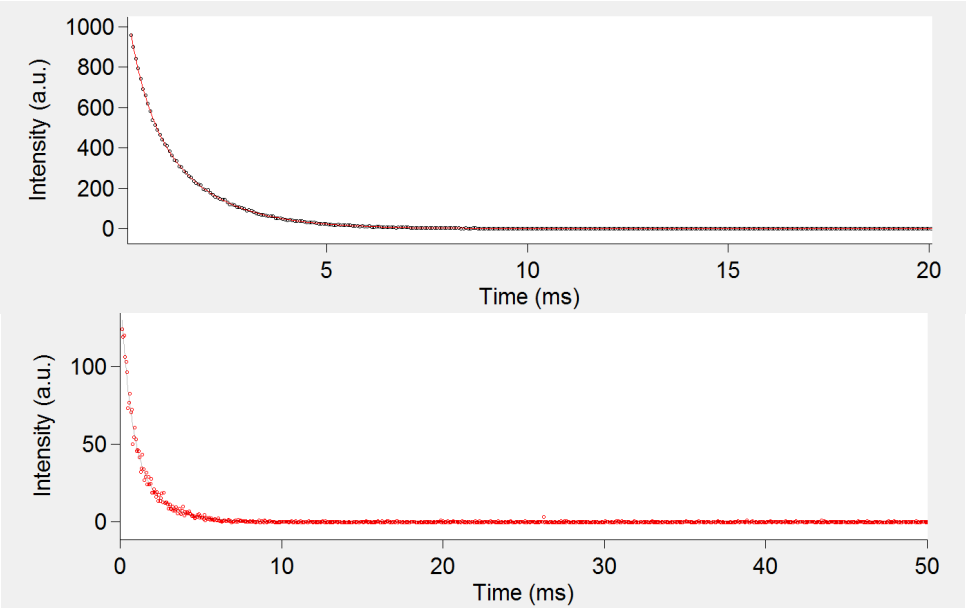

Figure S33. Lifetime of Eu(**1**)$_3$ complex fit with single exponential (Top) 616 nm (Bottom) 594 nm (0.01 mM, MeOH).

Table S1. Lifetime of Eu(**1**)$_3$ complex fit with single exponential (0.01 mM, MeOH).

Complex	Single Exponential (ms)	Average (ms)
Eu(**1**)$_3$ solution MeOH ($^5D_0 \rightarrow {}^7F_2$)	1.177	1.175
	1.168	
	1.179	
Eu(**1**)$_3$ solution MeOH ($^5D_0 \rightarrow {}^7F_1$)	1.055	1.059
	1.063	
	1.059	

Quantum Yields

Quantum yield measurements were determined by the dilute comparison method[2] using relative standards $Cs_3[Eu(dpa)_3]\cdot 8H_2O$, complex in a 0.1 M Tri-HCl buffer solution (pH ≈ 7.45) and quinine sulfate in 0.5 M H_2SO_4, with known quantum yields of Φ_{ref} = 24 ± 2.5 %, and Φ_{ref} = 0.546 % respectively.[3,4,5] $Cs_3[Eu(dpa)_3]\cdot 9H_2O$ was used for Eu(**1**)$_3$ and quinine sulfate was used for the 1,8-naphthalmide emission. Barrier slit widths remained the same between measurements for different compounds with 1.5, 3 nm excitation and emission widths. Excitation wavelength was the same for all measurements with the standard 279 nm excitation wavelength being used for Eu^{3+} emissions and 366 nm for quinine sulfate and 1,8-naphthalimide emissions. Complexes were dissolved in a 1:1 MeOH:CH_2Cl_2 and then diluted into MeOH.

Estimated overall quantum yields $\Phi_{Ln}^{L} = \Phi_x$ were calculated according to the following equation 1. Here grad refer to the slope of plotted emission area vs absorbance (emission area was taken from specific emission peaks, Eu(**1**)$_3$ ($^5D_0 \rightarrow {}^7F_2$), and 1,8-naphthalimide excimer and monomer broad emissions vs quinine sulfate), n refers to refractive index of the solution (a refractive index of n = 1.3295 was found for MeOH:CH_2Cl_2 solution), and subscript are ref for reference and x for sample.[3]

$$\boldsymbol{\Phi_x = \Phi_{std}\left(\frac{grad_x}{grad_{ref}} \times \left(\frac{n_x{}^2}{n_{ref}{}^2}\right)\right)} \ (\mathbf{1})$$

Radiative lifetime (τ^{rad}) of Eu(**1**)$_3$ was estimated by equation 2 which assumes that the magnetic dipole of Eu^{3+} ($^5D_0 \rightarrow {}^7F_1$) is independent of its coordination environment. [3] Abbreviations refer to; n for refractive index, $\frac{I_{MD}}{I_{tot}}$ is the ratio of area under the Eu^{3+} ($^5D_0 \rightarrow {}^7F_1$) to the integrated total emission (J=0-6), and $A_{MD,O}$ is the spontaneous emission probability of the Eu^{3+} ($^5D_0 \rightarrow {}^7F_1$) transition (14.65 s^{-1}). [3]

$$\tau^{rad} = \frac{1}{A_{MD,O}n^3}\left(\frac{I_{MD}}{I_{tot}}\right) \ (2)$$

From this intrinsic quantum yields (Φ_{Ln}^{Ln}) can be estimated with equation 3 using observed lifetime (τ_{obs}) and in turn used to find the sensitization efficiency (n_{sens}) with equation 4.[3]

$$\Phi_{Ln}^{Ln} = \frac{\tau_{obs}}{\tau^{rad}} \ (3)$$

$$n_{sens} = \frac{\Phi_{Ln}^{L}}{\Phi_{Ln}^{Ln}} \ (4)$$

Table S2. *Quantum yield results for Eu^{3+} centred emission.*

Complex	Φ_{Ln}^{L}	τ_{obs} (ms)	τ_{rad} (ms)	Φ_{Ln}^{Ln}	n_{sens}
Eu(**1**)$_3$	7.6 %	1.059	4.998	21.2 %	35.9 %

Table S3. Fluorescence *quantum yield results for 1,8-napthalimide centred emission.*

Complex	Φ_f
1H	12. 4 %
Eu(**1**)$_3$	15. 0 %
La(**1**)$_3$	15.0 %

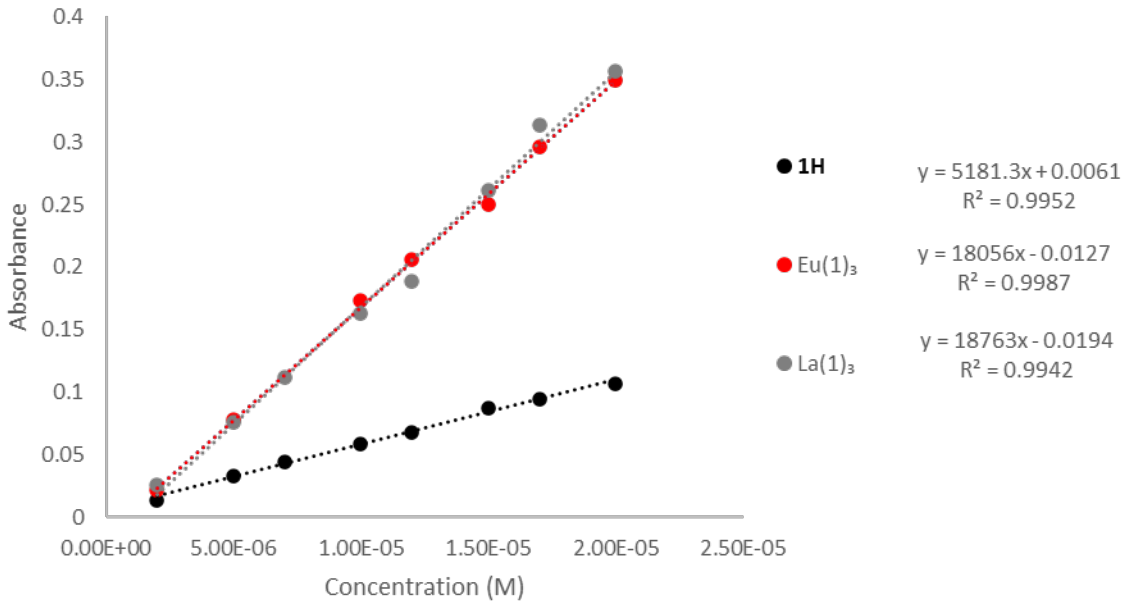

Figure S34. *Concentration vs absorbance for* ***1H****, Eu(****1****)₃ and La(****1****)₃ in MeOH.*

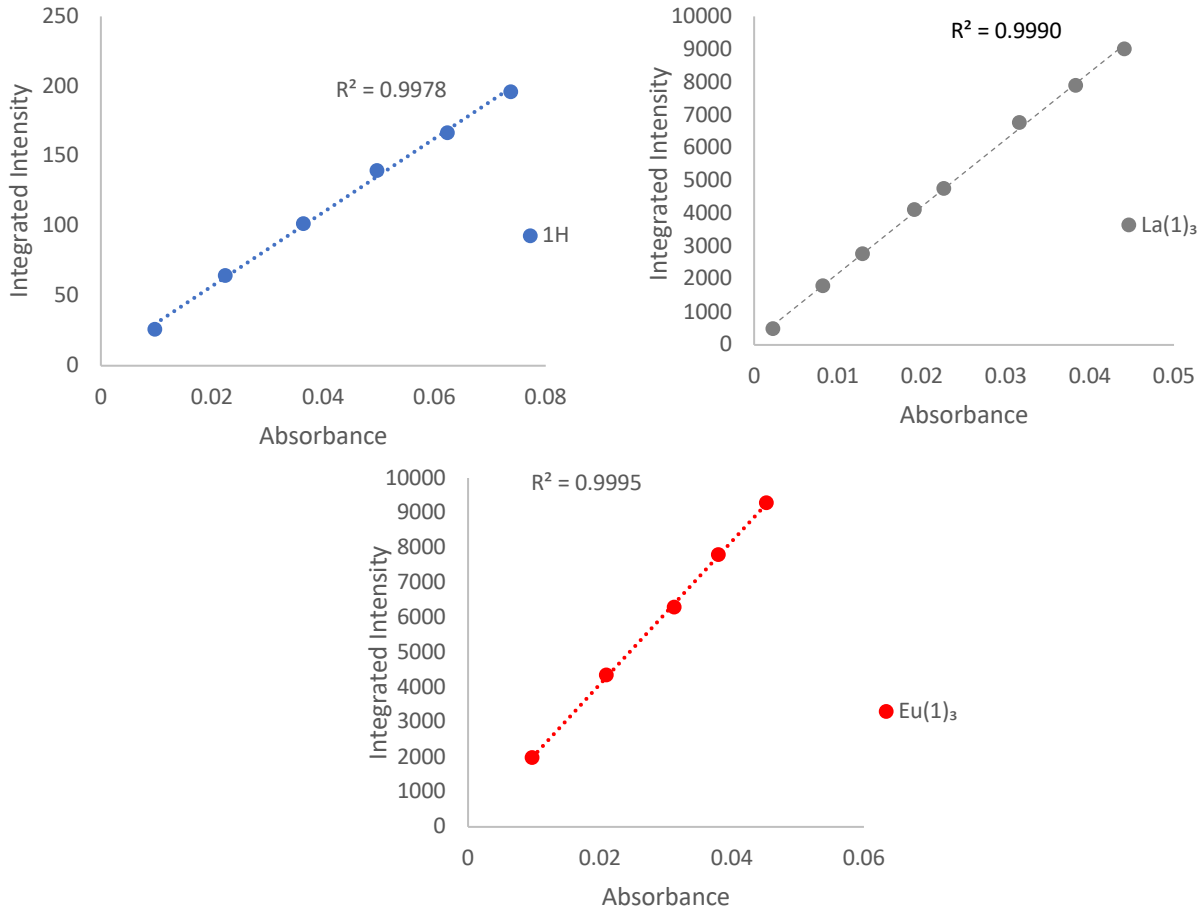

Figure S35. Integrated intensity vs absorbance of **1H**, Eu(**1**)$_3$ and La(**1**)$_3$ in MeOH (1.5 and 3 nm excitation and emission widths, λ_{ex} = 366 nm).

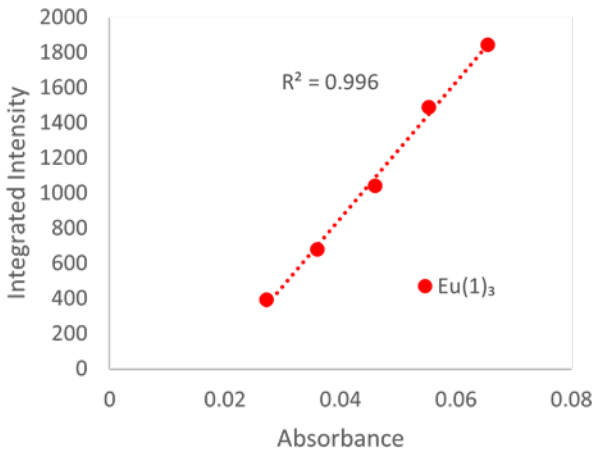

Figure S36. Integrated intensity vs absorbance of Eu(**1**)$_3$ in MeOH (1.5 and 3 nm excitation and emission widths, λ_{ex} = 279 nm).

Section 4 - Self-Assembly Titrations

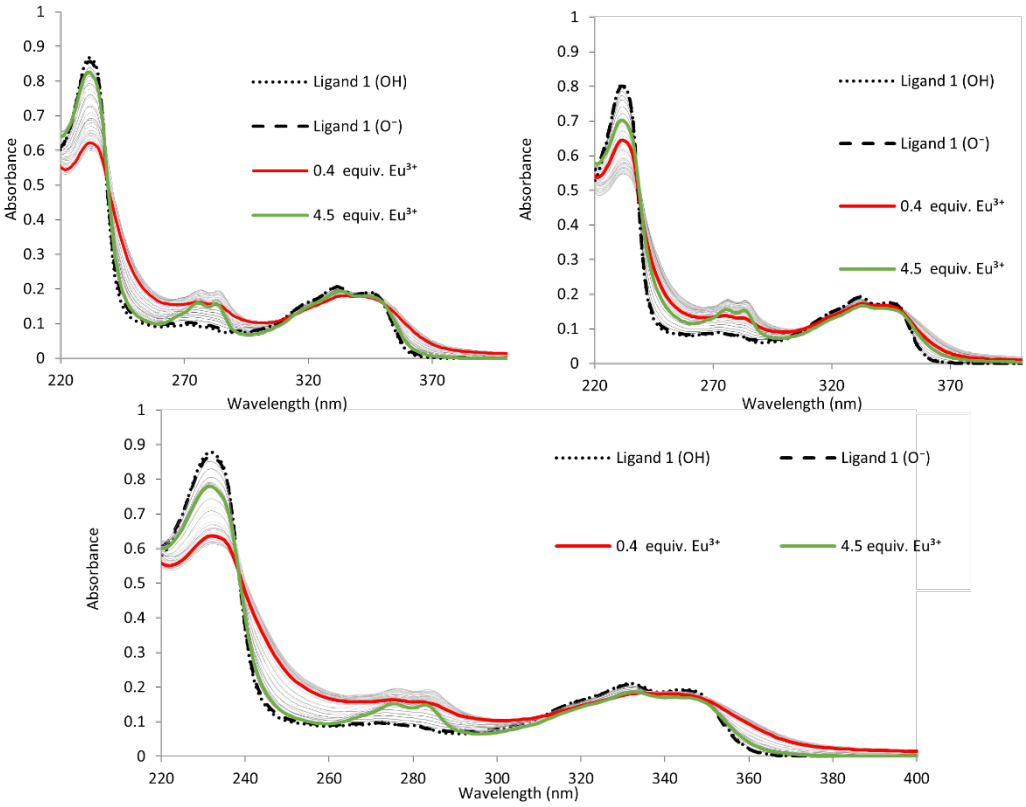

Figure S37. *UV-visible absorption titration of* ***1H*** *with $Eu(CF_3SO_3)_3$ from 0 to 4.5 equivalents, done in triplicate (0.02 mM, MeOH).*

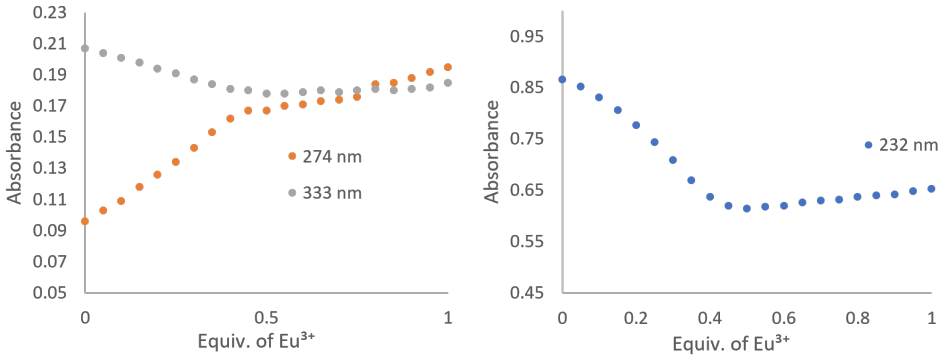

Figure S38. *Monitoring changes in UV-visible absorption spectra at specific wavelengths (232, 274 and 333 nm) during titration of* ***1H*** *(0.02 mM, MeOH) with $Eu(CF_3SO_3)_3$ from 0 to 1 equivalents.*

Section 5 - Colour-Tunable Emission

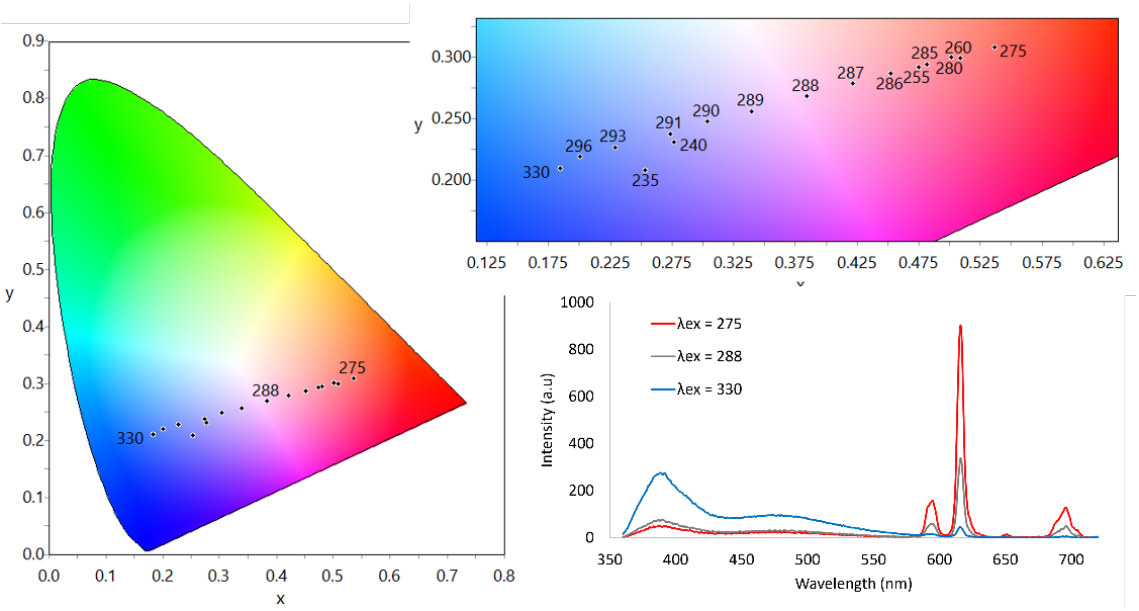

Figure S39. *CIE chromaticity diagram with different overall colours cable of Eu(**1**)$_3$ in a 0.01 mM MeOH solution dependent on λ_{ex} and fluorescence spectra at important λ_{ex}. Calculated 1931 CIE coordinates, 235 nm x,y = 0.25, 0.21; 240 nm x,y = 0.28 ,0.23; 255 nm x,y = 0.47, 0.29; 260 nm x,y = 0.51, 0.30; 275 nm x,y = 0.54, 0.30; 280-4 nm x,y = 0.50, 0.30; 285 nm x,y = 0.48, 0.29; 286 nm x,y = 0.45, 0.29; 287 nm x,y = 0.42, 0.28; 288 nm x,y = 0.38, 0.27; 289 nm x,y = 0.34, 0.26; 290 nm x,y = 0.30, 0.24; 291 nm x,y = 0.27, 0.24; 293 nm x,y = 0.23, 0.22; 296 nm x,y = 0.20, 0.22 and 330 nm x,y = 0.18, 0.20.*

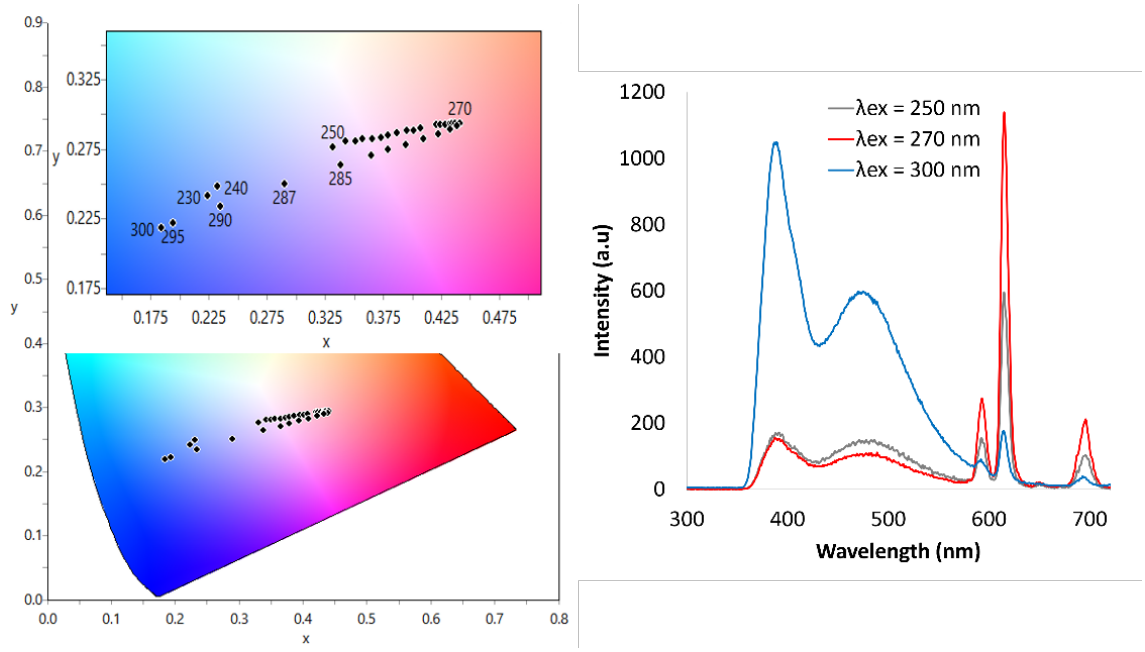

***Figure S40**. CIE chromaticity diagram with different overall colours capable of Eu(**1**)$_3$ in a 1 mM MeOH solution dependent on λ_{ex} and fluorescence spectra at important λ_{ex}. Calculated 1931 CIE coordinates, 230 nm x,y = 0.22, 0.24; 240 nm x,y = 0.23 ,0.25; 250 nm x,y = 0.33, 0.28; 251 nm x,y = 0.34, 0.28; 252 nm x,y = 0.35, 0.28; 253 nm x,y = 0.36, 0.28; 254 nm x,y = 0.37, 0.28; 255 nm x,y = 0.37, 0.29; 256 nm x,y = 0.38, 0.29; 257 nm x,y = 0.39, 0.29; 258-260 nm x,y = 0.40, 0.9; 261-264 nm x,y = 0.42, 0.29; 265-266 nm x,y = 0.43, 0.29; 267-275 nm x,y = 0.44, 0.29; 277 nm x,y = 0.42, 0.28; 280 nm x,y = 0.41, 0.28; 285 nm x,y = 0.34, 0.27; 290 nm x,y = 0.24, 0.24 and 300 nm x,y =0.18, 0.22.*

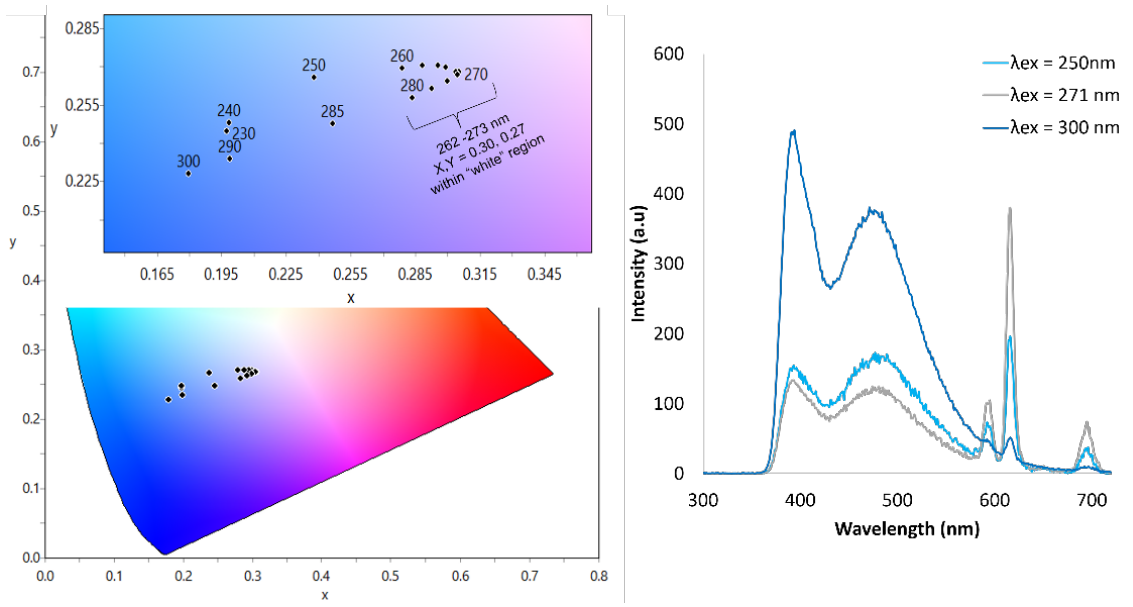

Figure S41. *CIE chromaticity diagram with different overall colours capable of Eu(**1**)$_3$ in a5 mM MeOH solution dependent on λ_{ex} and fluorescence spectra at important λ_{ex}. Calculated 1931 CIE coordinates, 230 nm x,y = 0.20, 0.25; 240 nm x,y = 0.20 ,0.25; 250 nm x,y = 0.24, 0.27; 260 nm x,y = 0.28, 0.27; 261 nm x,y = 0.28, 0.27; 261 nm x,y = 0.29, 0.27; 262-273 x,y = 0.30, 0.27; 275 nm x,y = 0.30, 0.26; 277 nm x,y = 0.29 ,0.26; 280 nm x,y = 0.28, 0.26 ; 285 nm x,y = 0.25, 0.25; 290 nm x,y = 0.20, 0.23 and 300 nm x,y = 0.18, 0.23.*

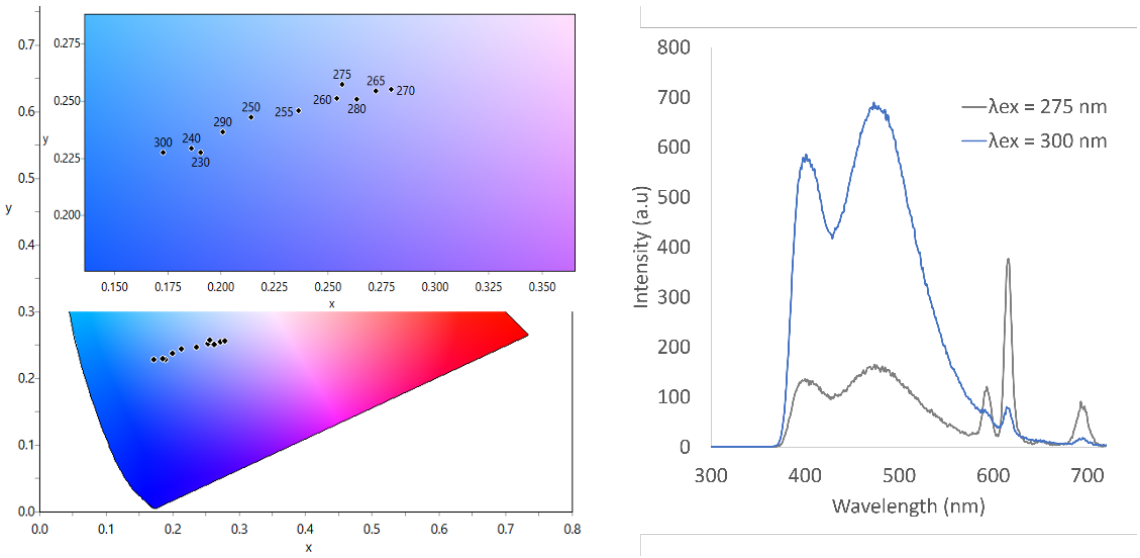

Figure S42.*CIE chromaticity diagram with different overall colours capable of Eu(**1**)$_3$ in a 10 mM MeOH solution dependent on λ_{ex} and fluorescence spectra at important λ_{ex}. Calculated 1931 CIE coordinates, 230 nm x,y = 0.19, 0.23; 240 nm x,y = 0.19 ,0.23; 250 nm x,y = 0.21, 0.24; 255 nm x,y = 0.24, 0.25; 260 nm x,y = 0.25, 0.25; 265nm x,y = 0.27, 0.26; 270 nm x,y = 0.28 ,0.26; 275 nm x,y = 0.26, 0.26 ; 280 nm x,y = 0.26, 0.28; 290 nm x,y = 0.20, 0.24 and 300 nm x,y = 0.17, 0.23..*

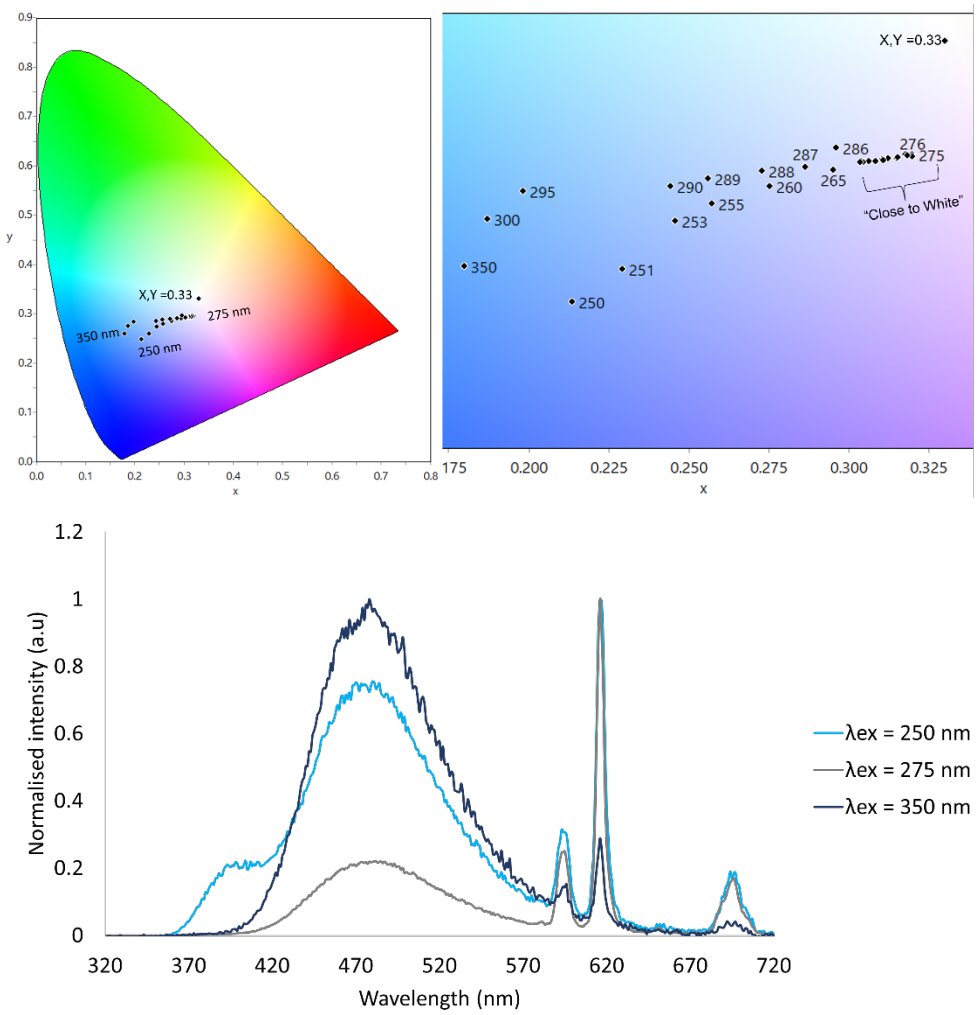

Figure S43. *(Top) CIE chromaticity diagram with different overall colours capable of solid Eu(**1**)$_3$ dependent on λ_{ex}. (Bottom) shows different fluorescence profiles of solid Eu(**1**)$_3$ at important excitation wavelengths. Calculated 1931 CIE coordinantes, 250 nm x,y = 0.21, 0.25; 251 nm x,y = 0.23 ,0.25; 253 nm x,y = 0.24, 0.27; 255 nm x,y = 0.26, 0.28; 260 nm x,y = 0.28, 0.29; 265 nm x,y = 0.39, 0.29; 270 nm x,y = 0.31 ,0.29; 271-272 nm x,y = 0.31, 0.29 ; 273-278 nm x,y = 0.32, 0.29; 278-280 nm x,y = 0.31, 0.29 ; 281-286 nm x,y = 0.30, 0.29; 287 nm x,y = 0.29, 0.29; 288 nm x,y = 0.28, 0.29; 289 nm x,y = 0.26, 0.29; 290 nm x,y = 0.24, 0.28; 295 nm x,y = 0.20, 0.28; 300 nm x,y = 0.19, 0.27; 310 nm x,y = 0.18, 0.26 and 350 nm x,y = 0.18,, 0.26;*

Section 6 - Spin Coated Films

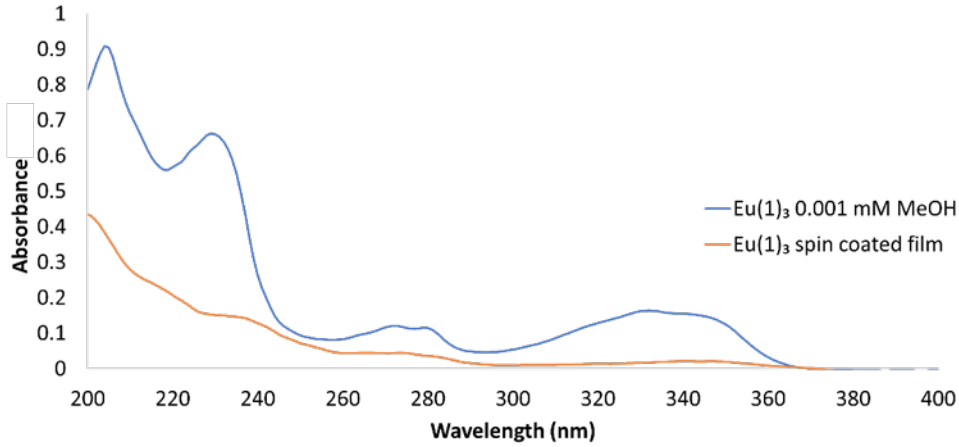

Figure S44. *UV-visible absorption spectra of spin coated Eu(**1**)$_3$ film and Eu(**1**)$_3$ solution (0.01 mM MeOH)*

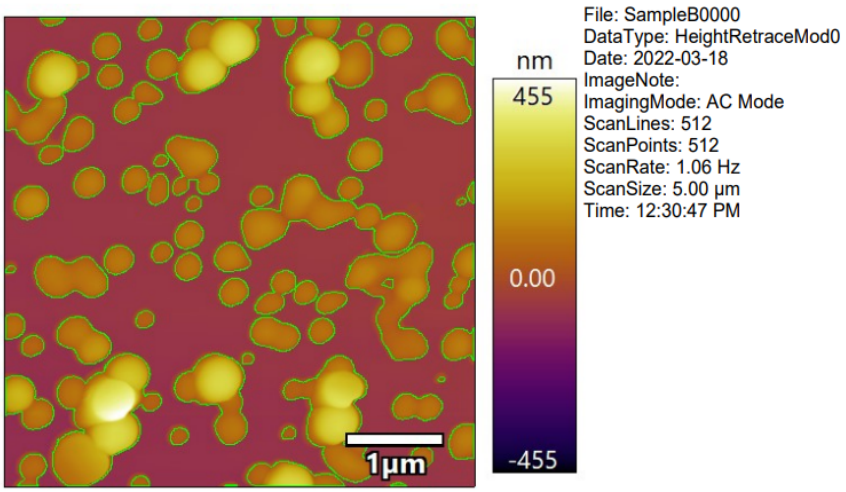

Figure S45. *AFM image of spin coated film with average particle height of 130 nm with a stdev 38 nm.*

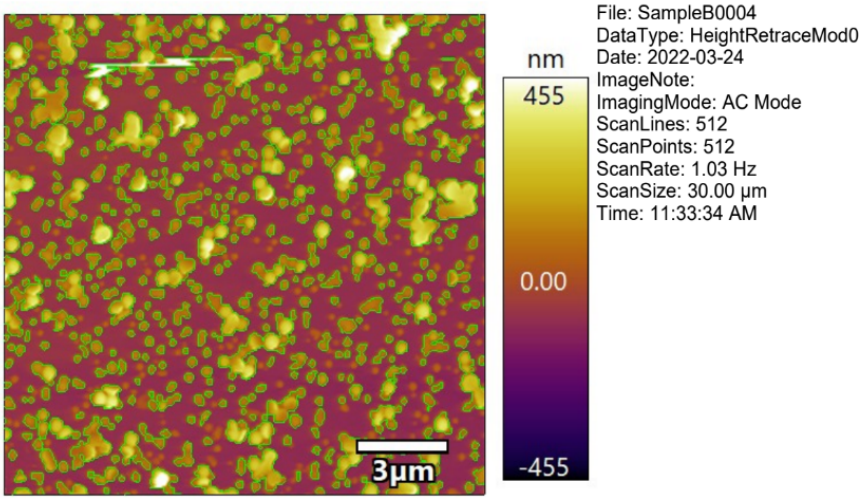

Figure S46. *AFM image of spin coated film with average particle height of 137 nm with a stdev 44 nm.*

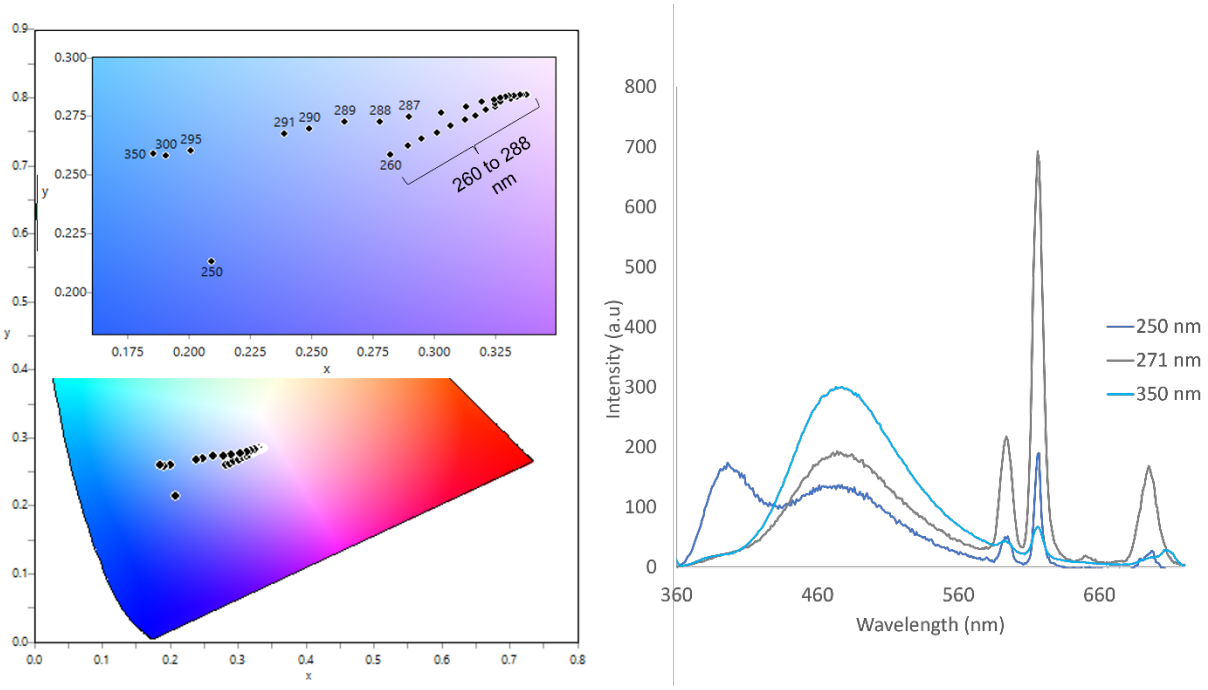

***Figure S47**. CIE chromaticity diagram with different overall colours capable of Eu(**1**)$_3$ in the 4000 rpm spin coated film dependent on λ_{ex} and fluorescence spectra of important λ_{ex}. Calculated 1931 CIE coordinates, 250 nm x,y = 0.21, 0.21; 260 nm x,y = 0.28, 0.26; 261 nm x,y = 0.29, 0.26; 262-263 nm x,y = 0.30, 0.27; 264-265 nm x,y = 0.31, 0.27; 266-269 nm x,y = 0.32, 0.28; 270-272 nm x,y = 0.33, 0.28; 273-278 nm x,y = 0.34, 0.28; 279-283 nm x,y = 0.33, 0.28; 284 nm x,y = 0.32, 0.28; 285 nm x,y = 0.31, 0.28; 286 nm x,y = 0.30, 0.28; 287 nm x,y = 0.29, 0.27; 288 nm x,y = 0.28, 0.27; 289nm x,y = 0.26, 0.27; 290 nm x,y = 0.25, 0.27; 295 nm x,y = 0.20, 0.26 and 300-350 nm x,y = 0.19, 0.26*

Section 7 - References

1. LED ColourCalculator (Version 7.7), OSRAM Sylvain, inc.
2. Crosby, G. A.; Demas, J. N., J. Phys. Chem. 1971, 75, 991-1024.
3. A. S. Chauvin, F. Gumy, D. Imbert and J. C. G. Bünzli, *Spectrosc. Lett*, 2004, **37**, 517-532.
4. A. S. Chauvin, F. Gumy, D. Imbert and J. C. G. Bünzli, *Spectrosc. Lett.*, 2007, **40**, 193-193.
5. A. Brouwer, *Pure Appl. Chem.*, 2011, **83**, 2213-2228.